pharmaceutics

MDPI

Review

Molecular Simulations of PEGylated Biomolecules, Liposomes, and Nanoparticles for Drug Delivery Applications

Hwankyu Lee

Department of Chemical Engineering, Dankook University, Yongin 16890, Korea; leeh@dankook.ac.kr

Received: 23 May 2020; Accepted: 8 June 2020; Published: 10 June 2020

Abstract: Since the first polyethylene glycol (PEG)ylated protein was approved by the FDA in 1990, PEGylation has been successfully applied to develop drug delivery systems through experiments, but these experimental results are not always easy to interpret at the atomic level because of the limited resolution of experimental techniques. To determine the optimal size, structure, and density of PEG for drug delivery, the structure and dynamics of PEGylated drug carriers need to be understood close to the atomic scale, as can be done using molecular dynamics simulations, assuming that these simulations can be validated by successful comparisons to experiments. Starting with the development of all-atom and coarse-grained PEG models in 1990s, PEGylated drug carriers have been widely simulated. In particular, recent advances in computer performance and simulation methodologies have allowed for molecular simulations of large complexes of PEGylated drug carriers interacting with other molecules such as anticancer drugs, plasma proteins, membranes, and receptors, which makes it possible to interpret experimental observations at a nearly atomistic resolution, as well as help in the rational design of drug delivery systems for applications in nanomedicine. Here, simulation studies on the following PEGylated drug topics will be reviewed: proteins and peptides, liposomes, and nanoparticles such as dendrimers and carbon nanotubes.

Keywords: PEGylation; molecular dynamics simulation; drug delivery; protein; peptide; liposome; dendrimer; carbon nanotube

1. Introduction

Polyethylene glycol (PEG) and polyethylene oxide (PEO), which are hydrophilic polymers composed of the subunit $-(CH_2-CH_2-O)_n-$, have been often covalently or noncovalently attached to the surfaces of drug molecules or transporters, a process called PEGylation [1,2]. PEG chains can sterically shield the encapsulated drugs from plasma proteins in the bloodstream and maintain good water solubility, leading to increased circulating lifetime and decreased cytotoxicity [3–9]. Therefore, the PEGylation method has been widely applied to pharmaceutical industries over the past three decades, since the first PEGylated protein was clinically approved by the FDA in the early 1990s [10,11]. Despite this successful application of PEGylation, the effects of PEG size, structure, and grafting density on the efficiency of drug delivery have not been well interpreted because of the limited resolution of experimental techniques. To complement experimental observations at nearly the atomic scale, molecular dynamics (MD) simulations have been performed. Figure 1 lists the number of publications on the development of PEG force fields (FFs) and MD simulations of PEGylated biomolecules and nanoparticles. Since all-atom and coarse-grained (CG) PEG FFs have been developed after 1995, short linear PEG chains were mainly simulated up until the 2000s, but recent advances in computer power and simulation methodologies have allowed many more simulations of large complexed (e.g., branched) PEG chains, PEGylated nanoparticle (or protein)-drug complexes and their self-assemblies interacting

with plasma proteins and lipid membranes [12–14]. In particular, simulations have revealed that PEGylation influences the conformations and surface properties of drug molecules or transporters and thus modulates the efficiency of drug delivery and release, which helps explain atomic-level phenomena and determine the optimal size, structure, and density of PEG for drug delivery applications [12,14]. Note that the conformation of PEGs and their interactions with other molecules can be reasonably predicted only in the presence of accurate FFs. For the development of all-atom [15–23] and CG models [24–31] for PEG and PEO, previous review papers are recommended [12–14].

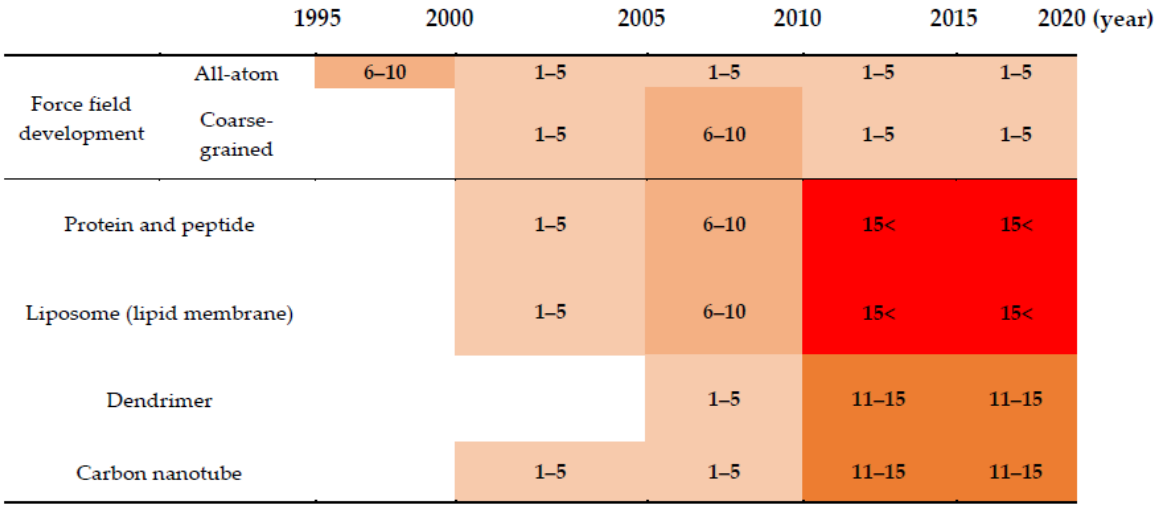

Figure 1. Number of publications on the force-field development and molecular dynamics simulations of polyethylene glycol (PEG)ylated biomolecules and nanoparticles (the numbers of publications, 1–5, 6–10, 11–15, and 15<, are represented in the order of light to dark red colors).

In this review, we will first (Section 2) review MD simulations of PEGylated biomolecules such as proteins, antimicrobial peptides (AMPs), and coiled coil peptides, focusing on their structural changes induced by PEGylation. Next (Section 3), MD simulations of PEGylated liposomes interacting with drugs and plasma proteins will be reviewed, which are interpreted by the polymer theory regarding the effect of PEG size and density on protein adsorption. Lastly (Section 4), we will focus on simulations of PEGylated nanoparticles such as dendrimers and carbon nanotubes (CNTs).

2. PEGylated Biomolecules: Proteins, Antimicrobial Peptides, and Coiled Coil Peptides

Since Abuchowski et al. found the effect of PEGylation on immunogenicity and circulating lifetime of serum albumin proteins in 1977 [32,33], PEGylated protein-based drugs or drug transporters have been clinically approved such as Neulasta [34], Oncaspar [35], Cimzia [36], Mircera [37], Omontys [38], Macugen [39], Plegridy [40], Krystexxa [41], Adagen, Pegasys, Sylatron, PEGIntron, Somavert [3,10,42,43]. Although PEGylation has been successfully applied for protein- and peptide-based pharmaceutics [7,44–46], the structural stability and surface properties of PEGylated proteins need to be understood to increase drug delivery efficiency. Since the structural change of proteins cannot be negligible, most simulation studies have been performed using all-atom models rather than CG models, although some CG simulations have shown the conformation of the grafted PEG. Here, PEGylated proteins, AMPs, and coiled coil peptides will be reviewed.

2.1. Proteins

Manjula et al. performed all-atom simulations of PEGylated hemoglobin and showed that PEG chains on the protein surface have the folded structure rather than the extended conformation, which weakens the interactions between hemoglobin and other biopolymers [47,48]. The Liu group simulated PEGylated insulin in water, showing that PEG chains do not only interact with hydrophobic

residues of insulin but also form hydrogen bonds with water, leading to the increased size and stability of insulin, which helps explain the longer circulating lifetime as observed in experiments [49]. They also investigated the interactions of PEG with lysozyme [50] and cytochrome c [51], showing the effect of PEGylation on the conformation and stability of proteins at different temperatures. Xue et al. simulated a series of five small peptides grafted with PEG, showing that PEGylation more significantly influences the conformations of charged peptides than those of neutral peptides [52]. Mu et al. showed that PEG size and PEG-conjugated position modulate the hydrodynamic volume of the Staphylokinase–PEG complex and the flexibility of grafted PEG chains [53]. Khameneh et al. simulated PEGylated human growth hormone with its receptor and performed the docking analysis, showing the random-coil formation of PEG and the reduced binding affinity between human growth hormone and its receptor in the presence of PEG [54]. The Accardo group simulated PEGylated hexa-phenylalanine [55,56], tetra-tryptophan [57], and tyrosine-containing aromatic peptides [58], showing the effect of PEGylation on the conformation and stability of assembled structures.

Recently, the interactions between PEG and individual amino acids have been quantified and applied to predict the extent of protein folding. Settanni et al. simulated a mixture of PEG and plasma proteins such as serum albumin, transferrin, complement Cq1, and apolipoprotein A1, and calculated the local density of PEG near individual amino acids, the preferential binding coefficient of each peptide for PEG [59,60], and the conformation and thickness of PEG layer adsorbed on the protein surface [61], showing that PEG–protein interactions can be quantified by a simple model in terms of the solvent-accessible surface area exposed by each amino acid type on the protein surface, favorably compared with experimental results obtained by label-free proteomic mass spectrometry. Kurinomaru et al. [62], Zaghmi et al. [63], and Sindhu et al. [64] found the effect of PEGylation on the structure, dynamics, and binding affinity of enzyme-therapeutic drugs such as α-amylase, glutamate dehydrogenase, and L-asparaginase, respectively. The Colina group reparameterized non-bonded potential parameters of the MARTINI CG PEG FF that was previously developed by Lee et al. [25] and Rossi et al. [26], which allows the accurate prediction of the interactions between PEG and proteins [65]. Using this CG model, they simulated PEG interacting with plasma proteins such as bovine serum albumin, human serum albumin, and apo-human serum transferrin, which reasonably predict the experimentally observed local densities of PEG around individual amino acids [65,66]. In particular, they simulated PEGylated chymotrypsin (a digestive enzyme), showing that PEG chains stabilize partially unfolded intermediates and even help the refolding to an active conformation, to an extent dependent on pH as described in Figure 2 [67], which supports the experimental hypothesis regarding the effect of PEG on protein folding and helps in the rational design of protein–polymer conjugates. They also observed the dependence of the PEG–peptide hydrogel interaction on peptide sequence and solvent condition [68].

2.2. *Antimicrobial Peptides*

AMPs are cationic amphipathic peptides composed of less than 50 amino acids that can be extracted from eukaryotic organisms for their defense mechanism [69]. Cationic AMPs selectively bind to anionic bacterial cell membranes rather than neutral human cell membranes and thus have been considered a promising possible antibiotics [70,71]. To achieve this, the high concentration of AMP is required, but AMP at high concentrations can nonspecifically attack human cells, leading to a decrease in the efficiency of specific targeting, which limits the application of AMP as antibiotics. To overcome this, PEGylation has been experimentally applied to AMPs such as nisin [72], magainin 2, tachyplesin I [73,74], KYE_28 [75], LL-37 [76] and synthetic AMPs (CaLL [77] and M33 [78]), showing decreased antimicrobial activity and increased solubility, which has motivated simulation studies on the interactions between AMP and PEG.

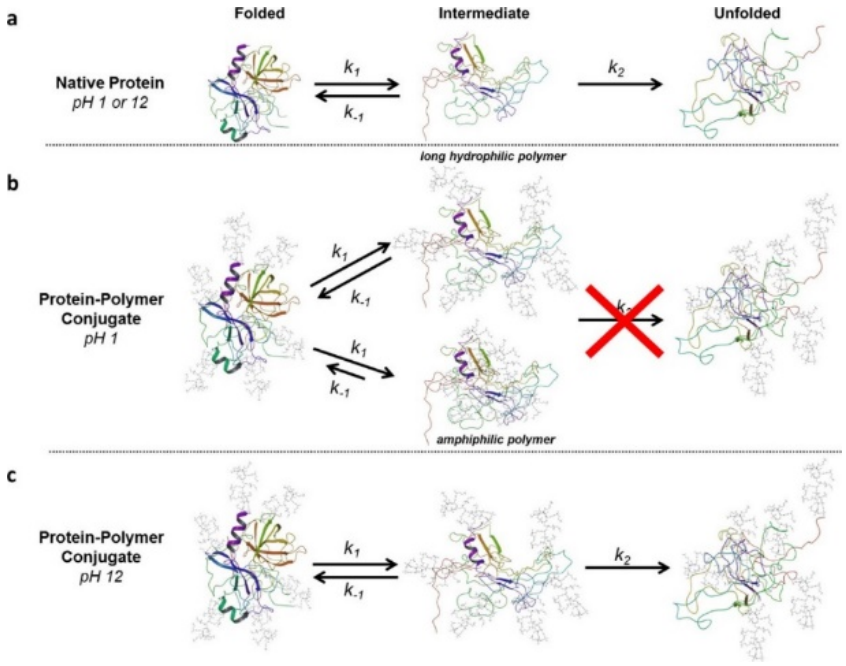

Figure 2. Unfolding pathways at different pH for (**a**) native chymotrypsin at pH 1 and 12, (**b**) PEGylated chymotrypsin at pH 1, and (**c**) PEGylated chymotrypsin at pH 12. PEG chains stabilize partially unfolded intermediate states and thus inhibit irreversible denaturation at pH 1 but not at pH 12 (reprinted with permission from [67]. Copyright (2018) American Chemical Society).

Wu et al. performed all-atom simulations of cecropin P1 grafted to the silica surface via a PEG cross-linker, showing the effect of PEG size and ionic strength on the conformation and antimicrobial activity of the peptide [79,80]. Our group simulated PEGylated magainin 2 and tachyplesin I interacting with lipid bilayers, showing that PEGylation reduces the binding strength between peptides and bilayer surfaces, which occurs more significantly for α-helical magainin 2 than for β-sheet tachyplesin I [81]. Recently, Jafari et al. simulated PEG-encapsulated magainin 2 and found that the PEG–peptide interaction is significantly modulated by aromatic and basic residues of the peptide [82], and Souza et al. simulated the insertion of PEG-encapsulated human beta-defensin-3 to lung surfactant models, showing that PEG chains promote the translocation of the peptide from gas phase to water phase [83]. Asadzadeh et al. simulated GF-17 (17th–32nd residues of LL-37) interacting with chitosan, PEG, or both, showing that the peptide interacts more tightly with PEG than with chitosan (Figure 3), leading to lower helicity in the presence of PEG [84].

2.3. Coiled Coil Peptides

Coiled coils are peptides composed of two or more α-helices wound into a superhelix. Sequences of coiled coils contain a heptad repeat of seven amino acid residues, where the 1st and 4th residues of each heptad repeat are hydrophobic [85]. These hydrophobic residues are located in the core of coiled coils and thus stabilize the superhelical structure of coiled coil bundles [85]. Coiled coils are found in approximately 10% of all proteins and serve critical roles as mediators of oligomerization of many proteins such as transcription factors, molecular motors, receptors and signaling molecules [86]. In addition, coiled coils can self-assemble to mechanically rigid protein fibers and thus have been synthesized for drug delivery applications as templates to promote the assembly of other molecules [87,88]. To increase their solubility and stability, PEGylated coiled coils have been experimentally synthesized by the Klok group [89–93], the Kros group [94–103], and the Xu group [104–113], showing membrane fusion and micelle assembly modulated by peptide sequence, PEG size and density, which have been theoretically complemented by simulations.

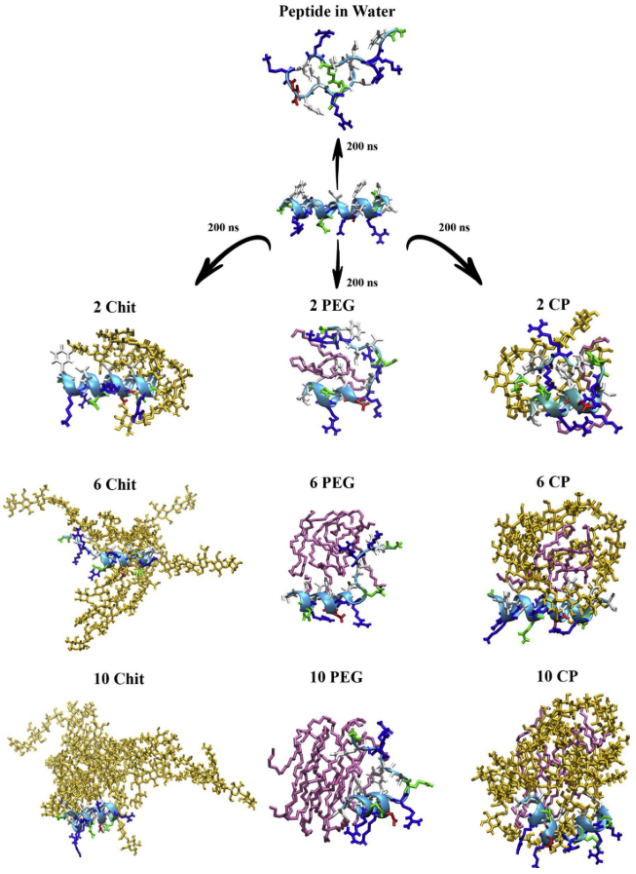

Figure 3. Snapshots of antimicrobial peptide GF-17 interacting with chitosan (**left**), PEG (**middle**), and both chitosan and PEG (**right**) (reprinted with permission from [84]. Copyright (2020) Elsevier).

Jain and Ashbaugh performed replica exchange simulations of PEGylated coiled coils, showing the higher helicity of coiled coils grafted with larger PEG chains due to the interactions between PEG and lysine residues of peptides [114]. The Keten group found strong interactions of PEG chains with both hydrophobic and polar residues of peptides, leading to increased helicity and decreased solvent-accessible surface area of the peptide in the presence of PEG, to an extent dependent on solvent hydrophobicity [115]. The binding energy of a cyclic peptide dimer was influenced by PEG length and grafting density [116]. They also found the high helicity and stability of coiled coils grafted with low-molecular weight PEG chains [117], and the extended structure of PEG chains grafted to helix micelles [110]. In particular, PEGylation influences the micelle size and stability, which is interpreted by a competition between the entropy of PEG conformations in the assembled state [111,118]. Recently, they performed both all-atom and CG simulations of PEGylated coiled coils composed of three or four helices, showing the formation of self-assembled micelles and the effect of the coiled coil oligomeric state on micelle size and stability [119]. Our group also performed all-atom and CG simulations of PEGylated trimeric coiled coils and their self-assembled micelles (Figure 4), and calculated their radii of gyration and hydrodynamic radii, which favorably compare with experimental values [120]. In particular, we found that hydrophobic residues in the exterior sites of coiled coils tend to be less exposed to water and thus interact with PEG, leading to the compact conformation of adsorbed PEG [120].

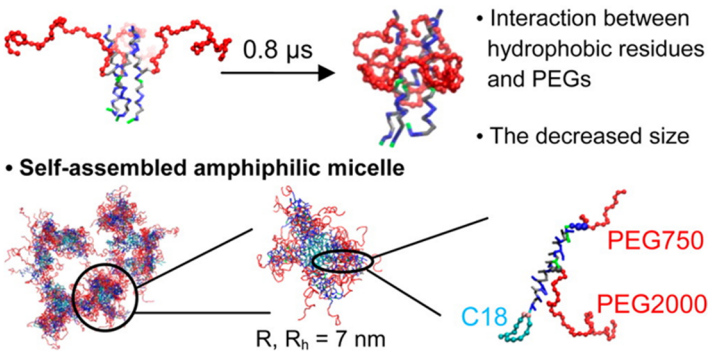

Figure 4. Initial and final snapshots of PEGylated trimeric coiled coils, showing the compact conformation of PEG due to the hydrophobic interaction (top). Snapshots of self-assembled micelles having a hydrodynamic radius of 7 nm for each micelle (bottom) (reprinted with permission from [120]. Copyright (2014) American Chemical Society).

3. PEGylated Liposomes

Liposomes, which are synthetic vesicles composed of phospholipid membranes, can transport drug molecules across specific cell membranes and thus have been widely used for drug delivery applications [121–123]. To increase solubility and circulating time of drug-encapsulating liposomes, PEG has been often attached to the liposome surface [2], since the first PEGylated liposomal doxorubicin (hydrophobic anticancer drug) was approved by the FDA in 1995 [124]. As the PEG size and concentration increase, encapsulated drug molecules can be more safely shielded from plasma proteins in the bloodstream, but also liposome membranes become unstable [125,126]. Therefore, many experiments have been performed to determine the maximum size and grafting density of PEG that can still maintain liposome stability [125,127–140], which has motivated theoretical studies on the effect of PEG size and grafting density on the conformation and dynamics of PEG chains grafted on the surface.

The Alexander–de Gennes theory has been applied to predict the transition of hydrophilic polymer chains between hemisphere (mushroom) and brush-like states on the surface [141]. Briefly, at very low grafting density, the grafted chain behaves like an isolated chain in solution, leading to a hemisphere (mushroom) conformation with a size given by the Flory radius, $R_F = aN^{3/5}$, where N is the degree of polymerization and a is the monomer size (Figure 5). At high grafting density ($D < R_F$), polymer chains become crowded and repel each other, leading to a brush-like conformation with a thickness given by $L = Na(a/D)^{2/3}$, where D is the distance between the grafting points of polymers. Jeon et al. calculated free energies of steric repulsion, van der Waals attraction, and hydrophobic interaction for the binding between spherical model proteins and PEO chains grafted on the hydrophobic surface, to an extent dependent on PEO length and grafting density [142]. Their free-energy calculations show that longer size and higher density (i.e., the brush state) lead to the optimal protein resistance, although surface density is more influential than chain length [142]. In particular, they determined optimal grafting densities of PEO for differently sized proteins, which was interpreted by steric repulsion and hydrophobic interaction between protein and PEO layer [143]. Szleifer also calculated free energies and showed the dependence of protein adsorption on the PEG density as well as on the protein conformation and concentration [144]. Halperin found that adsorption of small proteins can be repressed by increasing the grafting density, while adsorption of large proteins can be suppressed by increasing the brush thickness [145]. They also distinguish specific and nonspecific attractive interactions between various plasma proteins and PEG brushes [146]. Taylor and Jones found that the amount of proteins adsorbed onto PEGylated gold surfaces exponentially decreases as the brush density increases [147].

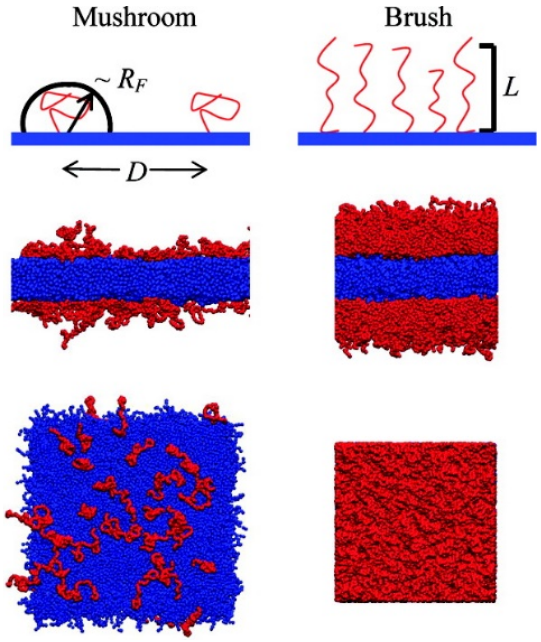

Figure 5. Schematic illustrations of the mushroom and brush conformations (**top**), and snapshots of the side (**middle**) and top-down (**bottom**) views at the end of simulations of PEG chains grafted on a hydrophobic surface (reprinted with permission from [25]. Copyright (2009) American Chemical Society).

To complement these theoretical models, MD simulations have been performed. The Roccatano group performed all-atom simulations of PEGylated lipid bilayers, and their free-energy calculations showed the strong interactions between PEG and lipid headgroups of bilayers [148,149]. Bunker and coworkers parameterized the all-atom PEG model and simulated PEGylated lipid bilayers, showing the interactions between PEG oxygens and Na^+ ions, and the penetration of PEG chains into a liquid-crystalline membrane but not into a gel-phased membrane [16]. They also found that the strength of the interaction between PEG and salt is modulated by PEG density, salt concentration and type such as NaCl, KCl, and $CaCl_2$ [150]. They simulated small peptides interacting with PEGylated lipid bilayers, showing the dependence of peptide penetration on hydrophobicity [151]. In particular, Na^+ ions bind to lipid bilayers and PEG chains grafted to drug molecules, which induces electrostatic repulsive interactions between lipid bilayers and PEGylated drugs [152]. PEGylation modulates the effect of cholesterol on the conformation and dynamics of lipid bilayers [153]. Their simulations also captured the insertion of hydrophobic drug or light-sensitizing molecules (e.g., porphyrins, indocyanine green, itraconazole, and piroxicam) to the PEG layer and the hydrophobic region of the bilayer (Figure 6) [154–158]. Recently, they simulated linear and branched PEG chains grafted on lipid bilayers, showing that the architecture and length of PEG–lipid conjugates influence the structure and dynamics of membranes, in agreement with experimental results [159].

Although all-atom simulations have captured the conformation and dynamics of PEGylated bilayers and their interactions with hydrophobic drug molecules and salt ions, the effects of PEG size and grafting density on liposome formation and protein adsorption have not been systematically simulated due to computational limitations of system size and time scale. To resolve this, the Klein group parameterized the CG model for PEG and PEGylated surfactants [160] and investigated the interactions between PEGylated surfactants and lipid bilayers [161] and the conformation of self-assembled PEGylated bicelles [162]. Our group also developed CG PEG model within the framework of the MARTINI FF [163,164], which lumps a monomer of PEG ($–(CH_2–CH_2–O)_n–$; three heavy atoms) into each CG bead [18,25]. This CG PEG model was further parameterized to increase dihedral stability by Rossi et al., showing the effect of PEGylation on the curvature of the surfactant bilayer [26].

Using this CG PEG model, Yang and Faller found that the presence of PEGylated lipid promotes the conformational transition from bilayers to micelles [165]. Hezaveh et al. developed another version of the MARTINI-based PEG model and showed the insertion of block copolymers into lipid bilayers, although their model does not include a dihedral potential and thus cannot reproduce the experimentally observed conformation of PEG chains in water [166].

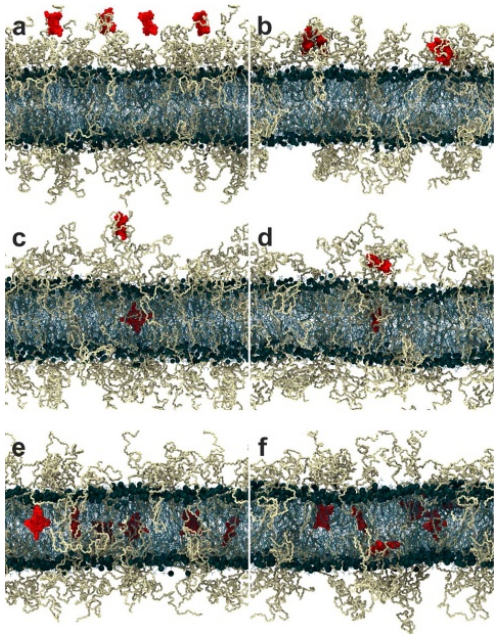

Figure 6. Snapshots of simulations showing the penetration of hydrophobic porphyrins into the PEGylated lipid bilayer as a function of time: four porphyrins at 0 ns (**a**) and 100 ns (**b**); two porphyrins at 0 ns (**c**) and 350 ns (**d**); six porphyrins at 0 ns (**e**) and 350 ns (**f**) (reprinted with permission from [154]. Copyright (2015) American Chemical Society).

Our group simulated a mixture of lipids and PEGylated lipids at different molar ratios, showing the formation of self-assembled liposomes, bicelles, and micelles, respectively, at 0–2.2, 10.5–27.4, and higher mol% of PEGylated lipid, in qualitative agreement with experiments [167]. This indicates that the phase behavior and size of lipid assemblies can be modulated by PEG density because their bulky headgroups increase membrane curvature [167]. Moreover, our CG simulations of PEG chains grafted to a nonadsorbing surface captured the conformational transition between brush and mushroom states, showing good agreement of simulation and Alexander–de Gennes theory [25]. In particular, we characterized the extent of protein adsorption to PEGylated lipid bilayers in terms of different PEG sizes (M_w = 750, 2000, and 5000) and grafting densities (1.6–25 mol%), showing that the binding between proteins and membranes is suppressed by the PEG layer in a brush but not in a mushroom (Figure 7), in quantitative agreement with the Alexander–de Gennes theory and experiments regarding much less adsorption of plasma proteins onto the membrane surface grafted with PEG in the brush state than in the mushroom state [168]. It is worth noting that the binding between plasma protein and bilayer surface can be predicted from the boundary between mushroom and brush states of PEG with different sizes and grafting densities, as highlighted in Figure 7. Recently, Sammalkorpi and coworkers showed the formation of self-assembled liposomes, bicelles, and micelles at different PEGylated-lipid concentrations [169,170], similar to our previous work [167].

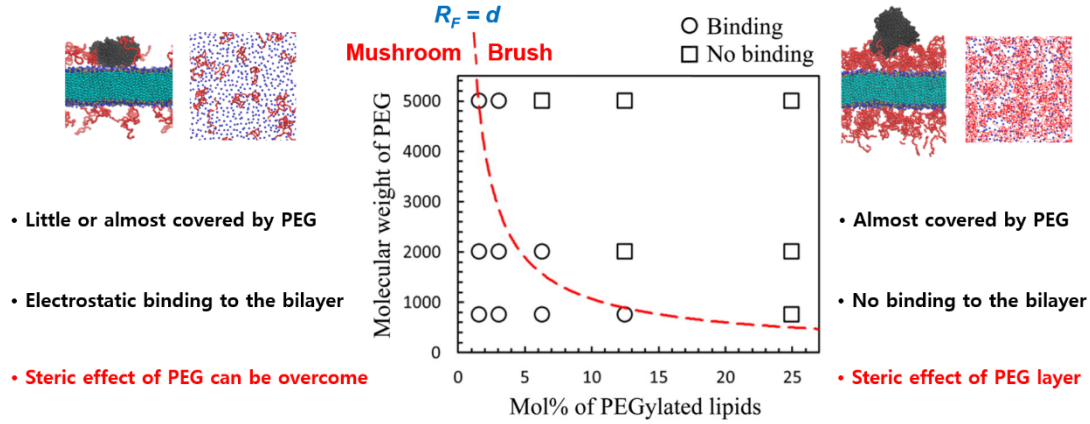

Figure 7. Characterization of binding (circles) and no-binding (squares) between plasma protein (human serum albumin) and the surface of PEGylated bilayer as functions of PEG size and grafting density. The boundary between mushroom and brush states is represented as a thick red line, where the Flory radius equals the distance between the grafting points of PEG (reprinted with permission from [168]. Copyright (2016) American Chemical Society).

4. PEGylated Nanoparticles

4.1. Dendrimers

Dendrimers, which consist of regularly branched monomeric building blocks with many surface terminal groups, have shown great potential for drug delivery applications because of their controlled mass, surface valency, and surface functionality [171]. Drug molecules can be either conjugated to the terminal group of dendrimer or encapsulated into the inner vacancy of dendrimer and then delivered to the desired site [172]. However, charged dendrimers have nonspecific interactions with cell membranes and thus have been neutralized by acetylating their surface terminals. In addition, PEG chains have been often attached to the dendrimer surface, which does not only decrease nonspecific cytotoxicity but also increases dendrimer solubility [173]. In particular, PEG can sterically shield drug molecules from plasma proteins in the bloodstream and thus increase their circulation lifetime [174], which has motivated many simulation studies on the conformation of PEGylated dendrimers and their interaction with drugs, proteins, and lipid membranes.

Tanis and Karatasos performed all-atom simulations of a dendrimer grafted with a single PEO chain, showing the effect of pH on the conformation of PEO and its hydrogen-bond interaction with dendrimer [175]. Karatosas also simulated the complex of PEGylated hyperbranched polyesters and doxorubicin, showing the effects of PEG size and doxorubicin charge on the hydrogen-bond interactions between PEGylated polyesters and doxorubicin [176]. Our CG simulations showed that PEGylation induces interparticle dispersion [177] and the lower extent of cytotoxicity and membrane permeability than acetylation does [178]. In particular, we found that longer chains with higher grafting densities promote PEG–PEG crowding and thus stretch dendrimer terminals towards water, leading to a larger dendrimer with a dense-shell structure [179]. Albertazzi et al. simulated dendrimers containing 2- and 4-arm PEG cores, showing more swollen conformation of dendrimer at higher concentrations of PEG core [180]. Their metadynamics simulations also showed that PEGylated dendrimers have a tight globular shape rather than an open conformation [181]. Pearson et al. showed conformational changes of PEGylated dendrimers at different charge densities [182], and Lin et al. found that PEGylated dendrimers adsorb to lipid monolayers but do not significantly influence the structure and properties of monolayers [183].

Recently, large complexes of PEGylated dendrimers and proteins (or drugs) have been simulated. Lim et al. [184] and Barraza et al. [185] respectively simulated paclitaxel and methotrexate drugs interacting PEGylated dendrimers, showing that PEG–PEG crowding decreases the extent of drug release, which helps determine the size and density of PEG for optimal drug release.

Sampogna-Mireles et al. simulated dendrimers grafted with PEG and folic acid, showing that PEG chains do not reduce the binding affinity between folic acid and folate receptor (Figure 8) [186], which should be highlighted because their simulations captured the effect of PEG on the binding affinity to the receptor protein. Hsu et al. simulated PEGylated dendron micelle and serum albumin, showing that the penetration of serum albumin into the micelle core can be suppressed by PEGylation [187]. Diaz et al. compared the conformations of dendrimers grafted with PEG or folic acid, showing different effects of PEG and folic acid on dendrimer size, which helps explain the experimentally observed relationship between dendrimer size and circulation time [188]. Wang et al. found that PEGylation significantly weakens the binding between dendrimers and plasma proteins such as human serum albumin and immunoglobulin [189]. Overall, the conformation of PEG and its effect on the internal structure of dendrimer were mainly studied until early 2010s, while the effect of PEGylation on the binding affinity to proteins and drug release efficiency have been more focused for the past five years.

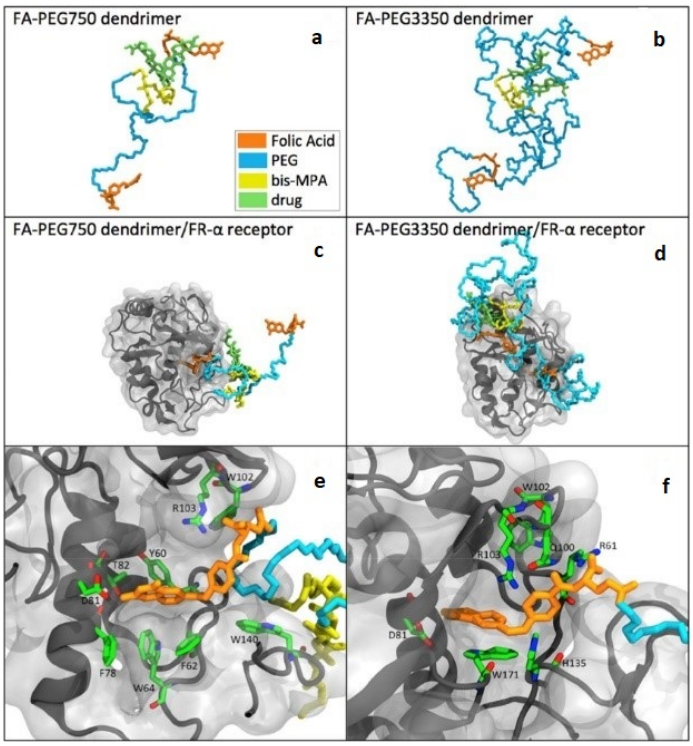

Figure 8. Snapshots of dendrimers complexed with drug, folic acid, and PEG ((**a**) PEG750 and (**b**) PEG3350), and those interacting with a folate receptor (**c**–**f**). (Reprinted with permission from [186]. Copyright (2017) Elsevier).

4.2. Carbon Nanotubes

Since CNTs are mechanically strong and chemically stable, they have been considered to be good candidate nanomaterials for use as drug transporters [190–192]. However, CNTs are highly hydrophobic and thus immediately aggregate in aqueous environment, which limits the application of CNTs at the physiological condition. To overcome this, PEG chains have been covalently or noncovalently attached to the CNT surface. Experiments have revealed the conformation and interparticle dispersion of PEGylated CNTs and their interactions with membranes, proteins, and drug molecules [193–200], which has motivated simulation studies.

In the early 2010s, most simulation studies focused on the conformation of PEG chains and their interactions with the CNT surface. Uddin et al. performed all-atom simulations of CNTs with a mixture of PEO and water, and their free-energy calculations showed the weak adsorption of PEO onto the CNT surface, which were explained by entropic and enthalpic contributions [201]. Our group

simulated random adsorption of PEGylated lipids onto the CNT surface [202] and found the effects of PEG size and grafting density on the conformation of PEG grafted onto CNT [203], which favorably compares with the transition of mushroom and brush states in the Alexander–de Gennes theory [141]. Di Crescenzo et al. simulated CNTs interacting with PEG (homopolymer) or PEG–propylene sulfide (PPS) block copolymers and found the stronger interaction of CNT with PEG–PPS than with PEG and the parallel arrangement PEG chains along the tube axis [204]. Aslan et al. compares density profiles of PEGylated lipids adsorbed onto isolated and bundled CNTs, which helps explain their different extents of antimicrobial activity [205]. Sarukhanyan et al. [206] and Han et al. [207] simulated CNTs interacting with various polymers, showing the effect of polymer hydrophobicity on the CNT-polymer conformation and interparticle dispersion. Maatta et al. found the dependence of CNT dispersion on PEG length and CNT diameter [208].

Recently, large complexes of PEGylated CNTs and other molecules such as lipid membranes, plasma proteins, and anticancer drug molecules have been simulated using all-atom and CG models. Skandani and Al-Haik showed slower penetration of PEGylated CNT into the lipid bilayer than unPEGylated CNT, which was explained by lower adhesion energy of PEGylated CNT [209], as observed in their previous experiments [210]. Our group showed interparticle dispersion and membrane curvature induced by PEGylated CNT [211], and the effects of protein shape, PEG size and grafting density on the adsorption of proteins onto PEGylated CNT [212]. Lin et al. investigated the binding affinity between CNTs and PEGylated proteins such as hormones, neurotransmitter, and vitamin [213], and Hashemzadeh and Raissi showed the adsorption of paclitaxel onto the PEGylated CNT [214]. Kavyani et al. compared the binding strength of CNTs with PEGylated and unPEGylated dendrimers, showing the stronger interactions of CNTs with PEGylated dendrimers than with unPEGylated dendrimers [215]. The Panczyk group performed all-atom simulations of PEGylated and folic acid-functionalized CNTs that encapsulate doxorubicin, showing the release of doxorubicin from CNTs at acidic pH but not at neutral pH [216]. Fullerene molecules were also included to the inner cavity of CNT functionalized with PEG and folic acid, where fullerenes act as magnetic pistons at acidic pH, leading to an increase in the release of doxorubicin from nanotube [217], which helps explain the effect of PEG on the efficiency of drug release as well as suggests the use of fullerene, as presented in Figure 9. Meran et al. simulated CNTs coated with PEGylated pyrene and showed the adsorption of PEGylated pyrene onto the CNT surface via π-π stacking interactions, which does not significantly depend on PEG length and CNT size [218]. Saberinasab et al. performed quantum-mechanics (QM) calculations and all-atom MD simulations of a mixture of PEGylated CNTs and Temozolomide (anticancer drug), showing the adsorption of Temozolomide on PEGylated CNT because of strong hydrogen-bond interactions [219]. Moradnia et al. also performed QM calculations and all-atom MD simulations of a mixture of PEGylated CNTs and Gemcitabine (anticancer drug), showing the effect of PEG size on the hydrogen-bond interactions of Gemcitabine with PEGylated CNT and water [220]. Overall, simulation studies focused on the conformation of PEG and its effect on CNT dispersion until the mid-2010s, but have recently focused more closely on the effect of PEGylation on the efficiency of drug release and the binding affinity to drugs and proteins.

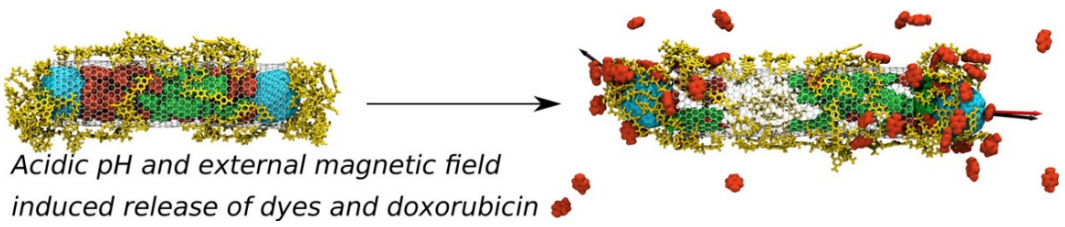

Figure 9. Snapshots of simulations of the carbon nanotubes (CNT) functionalized with PEGylated folic acid (yellow). Doxorubicin (green) and fullerene (light blue) were initially located in the inner cavity of CNT. After 1.5 ns of simulations, doxorubicin molecules are released from CNT at acidic pH but not at neutral pH (reprinted with permission from [217]. Copyright (2018) American Chemical Society).

5. Conclusions

All-atom and CG MD simulations have revealed much useful information about the structure and dynamics of PEGylated drug transporters such as proteins, peptides, liposomes, dendrimers, and CNTs, which cannot be easily captured by experiments. In 1995–2000s, all-atom and CG PEG FFs have been developed and used for simulations of short linear PEG and their interactions with small molecules and solvents, while recent advances in computer power and simulation methods have allowed simulations of large complexes of PEGylated drug carries and their interactions with anticancer drugs, plasma proteins, lipid membranes, and receptors.

Although the molecular simulation has proven to be a powerful tool for the in silico design of PEGylated drugs for the past two decades, there are still problems that need to be considered for the future work. Firstly, biological complexes, reaction kinetics and mass transport conditions of experiments and simulations differ, which precludes any quantitative comparison between simulations and experiments. For instance, there are hundreds of plasma proteins that flow through the bloodstream, and hundreds of membrane proteins that control cellular behavior and interactions with drug carriers. Recently, MD simulations start to simulate the corona formation of various plasma proteins [221] and human cell membranes composed of 63 different lipid species [222], showing promising efforts in mimics of biological systems. Secondly, more accurate FFs need to be developed to predict the interactions between PEG and other molecules such as nucleotides and amino acids. As reviewed above, all-atom and CG PEG FFs have accurately predicted the conformation and physical properties of PEG in solvent, but the prediction of their interactions with other molecules need to be improved. Lastly, large complexes of PEGylated drugs interacting with other molecules should be considered. This can be done by multiscale simulations of the transition between all-atom and CG models [223], where the conformation and dynamics can be equilibrated by CG simulations, and then CG coordinates can be converted to all-atom models that offer insights into the atomic-level interactions such as electrostatic, hydrophobic, and hydrogen-bond interactions. To achieve this, simulation methodologies need to be developed for the transition from CG to an all-atom model that can be compatible with various biomolecules, polymers, surfactants, and solvents.

Despite these limitations, MD simulations have successfully interpreted experimental observations at nearly the atomic scale and determined the optimal size, structure, and grafting density of PEG. Moreover, an increase in computational speed and methodology development (e.g., multiscale simulations of the transition between all-atom and CG models) will allow for more realistic simulations of larger biological systems, leading to a promising tool for the rational design of highly efficient PEGylated drug delivery systems.

Funding: This research received no external funding.

Conflicts of Interest: The authors declare no conflict of interest.

References

1. Harris, J.M.; Chess, R.B. Effect of pegylation on pharmaceuticals. *Nat. Rev. Drug Discov.* **2003**, *2*, 214–221. [CrossRef]
2. Harris, J.M.; Martin, N.E.; Modi, M. Pegylation—A novel process for modifying pharmacokinetics. *Clin. Pharmacokinet.* **2001**, *40*, 539–551. [CrossRef]
3. Veronese, F.M.; Pasut, G. PEGylation, successful approach to drug delivery. *Drug Discov. Today* **2005**, *10*, 1451–1458. [CrossRef]
4. Allen, T.M.; Hansen, C. Pharmacokinetics of Stealth Versus Conventional Liposomes—Effect of Dose. *Biochim. Biophys. Acta* **1991**, *1068*, 133–141. [CrossRef]
5. Allen, T.M.; Hansen, C.; Martin, F.; Redemann, C.; Yauyoung, A. Liposomes Containing Synthetic Lipid Derivatives of Poly(Ethylene Glycol) Show Prolonged Circulation Half-Lives Invivo. *Biochim. Biophys. Acta* **1991**, *1066*, 29–36. [CrossRef]

6. Maruyama, K.; Yuda, T.; Okamoto, A.; Ishikura, C.; Kojima, S.; Iwatsuru, M. Effect of Molecular-Weight in Amphipathic Polyethyleneglycol on Prolonging the Circulation Time of Large Unilamellar Liposomes. *Chem. Pharm. Bull.* **1991**, *39*, 1620–1622. [CrossRef] [PubMed]
7. Delgado, C.; Francis, G.E.; Fisher, D. The uses and properties of peg-linked proteins. *Crit. Rev. Ther. Drug Carr. Syst.* **1992**, *9*, 249–304.
8. Maruyama, K.; Yuda, T.; Okamoto, A.; Kojima, S.; Suginaka, A.; Iwatsuru, M. Prolonged circulation time invivo of large unilamellar liposomes composed of distearoyl phosphatidylcholine and cholesterol containing amphipathic poly(ethylene glycol). *Biochim. Biophys. Acta* **1992**, *1128*, 44–49. [CrossRef]
9. Duncan, R. Polymer conjugates as anticancer nanomedicines. *Nat. Rev. Cancer* **2006**, *6*, 688–701. [CrossRef] [PubMed]
10. Turecek, P.L.; Bossard, M.J.; Schoetens, F.; Ivens, I.A. PEGylation of Biopharmaceuticals: A Review of Chemistry and Nonclinical Safety Information of Approved Drugs. *J. Pharm. Sci.* **2016**, *105*, 460–475. [CrossRef]
11. Knop, K.; Hoogenboom, R.; Fischer, D.; Schubert, U.S. Poly(ethylene glycol) in drug delivery: Pros and cons as well as potential alternatives. *Angew. Chem. Int. Ed.* **2010**, *49*, 6288–6308. [CrossRef] [PubMed]
12. Sousa, S.F.; Peres, J.; Coelho, M.; Vieira, T.F. Analyzing PEGylation through Molecular Dynamics Simulations. *ChemistrySelect* **2018**, *3*, 8415–8427. [CrossRef]
13. Rossi, G.; Monticelli, L. Modeling the effect of nano-sized polymer particles on the properties of lipid membranes. *J. Phys. Condens. Matter* **2014**, *26*, 503101. [CrossRef] [PubMed]
14. Lee, H. Molecular modeling of PEGylated peptides, dendrimers, and single-walled carbon nanotubes for biomedical applications. *Polymers* **2014**, *6*, 776–798. [CrossRef]
15. Bedrov, D.; Borodin, O.; Smith, G.D. Molecular dynamics simulations of 1,2-dimethoxyethane/water solutions. 1. Conformational and structural properties. *J. Phys. Chem. B* **1998**, *102*, 5683–5690. [CrossRef]
16. Stepniewski, M.; Pasenkiewicz-Gierula, M.; Rog, T.; Danne, R.; Orlowski, A.; Karttunen, M.; Urtti, A.; Yliperttula, M.; Vuorimaa, E.; Bunker, A. Study of PEGylated lipid layers as a model for PEGylated liposome surfaces: Molecular dynamics simulation and langmuir monolayer studies. *Langmuir* **2011**, *27*, 7788–7798. [CrossRef] [PubMed]
17. Vorobyov, I.; Anisimov, V.M.; Greene, S.; Venable, R.M.; Moser, A.; Pastor, R.W.; MacKerell, A.D. Additive and classical drude polarizable force fields for linear and cyclic ethers. *J. Chem. Theory Comput.* **2007**, *3*, 1120–1133. [CrossRef] [PubMed]
18. Lee, H.; Venable, R.M.; MacKerell, A.D.; Pastor, R.W. Molecular dynamics studies of polyethylene oxide and polyethylene glycol: Hydrodynamic radius and shape anisotropy. *Biophys. J.* **2008**, *95*, 1590–1599. [CrossRef] [PubMed]
19. Dong, H.; Hyun, J.K.; Durham, C.; Wheeler, R.A. Molecular dynamics simulations and structural comparisons of amorphous poly(ethylene oxide) and poly(ethylenimine) models. *Polymer* **2001**, *42*, 7809–7817. [CrossRef]
20. Tritopoulou, E.A.; Economou, I.G. Molecular simulation of structure and thermodynamic properties of pure tri- and tetra-ethylene glycols and their aqueous mixtures. *Fluid Phase Equilibria* **2006**, *248*, 134–146. [CrossRef]
21. Winger, M.; De Vries, A.H.; Van Gunsteren, W.F. Force-field dependence of the conformational properties of α, ω-dimethoxypolyethylene glycol. *Mol. Phys.* **2009**, *107*, 1313–1321. [CrossRef]
22. Neyertz, S.; Brown, D.; Thomas, J.O. Molecular dynamics simulation of crystalline poly(ethylene oxide). *J. Chem. Phys.* **1994**, *101*, 10064–10073. [CrossRef]
23. Lin, B.; Boinske, P.T.; Halley, J.W. A molecular dynamics model of the amorphous regions of polyethylene oxide. *J. Chem. Phys.* **1996**, *105*, 1668–1681. [CrossRef]
24. Srinivas, G.; Discher, D.E.; Klein, M.L. Self-assembly and properties of diblock copolymers by coarse-grain molecular dynamics. *Nat. Mater.* **2004**, *3*, 638–644. [CrossRef] [PubMed]
25. Lee, H.; de Vries, A.H.; Marrink, S.J.; Pastor, R.W. A Coarse-Grained Model for Polyethylene Oxide and Polyethylene Glycol: Conformation and Hydrodynamics. *J. Phys. Chem. B* **2009**, *113*, 13186–13194. [CrossRef]
26. Rossi, G.; Fuchs, P.F.J.; Barnoud, J.; Monticelli, L. A coarse-grained MARTINI model of polyethylene glycol and of polyoxyethylene alkyl ether surfactants. *J. Phys. Chem. B* **2012**, *116*, 14353–14362. [CrossRef]
27. Choi, E.; Mondal, J.; Yethiraj, A. Coarse-grained models for aqueous polyethylene glycol solutions. *J. Phys. Chem. B* **2014**, *118*, 323–329. [CrossRef]

28. Wang, Q.; Keffer, D.J.; Nicholson, D.M. A coarse-grained model for polyethylene glycol polymer. *J. Chem. Phys.* **2011**, *135*. [CrossRef] [PubMed]
29. Chen, T.; Hynninen, A.P.; Prud'homme, R.K.; Kevrekidis, I.G.; Panagiotopoulos, A.Z. Coarse-Grained Simulations of Rapid Assembly Kinetics for Polystyrene-b-poly(ethylene oxide) Copolymers in Aqueous Solutions. *J. Phys. Chem. B* **2008**, *112*, 16357–16366. [CrossRef]
30. Fischer, J.; Paschek, D.; Geiger, A.; Sadowski, G. Modeling of Aqueous Poly(oxyethylene) Solutions. 2. Mesoscale Simulations. *J. Phys. Chem. B* **2008**, *112*, 13561–13571. [CrossRef] [PubMed]
31. Bedrov, D.; Ayyagari, C.; Smith, G.D. Multiscale modeling of poly(ethylene oxide)-poly(propylene oxide)-poly(ethylene oxide) triblock copolymer micelles in aqueous solution. *J. Chem. Theory Comput.* **2006**, *2*, 598–606. [CrossRef] [PubMed]
32. Abuchowski, A.; McCoy, J.R.; Palczuk, N.C.; van Es, T.; Davis, F.F. Effect of covalent attachment of polyethylene glycol on immunogenicity and circulating life of bovine liver catalase. *J. Biol. Chem.* **1977**, *252*, 3582–3586. [PubMed]
33. Abuchowski, A.; Van Es, T.; Palczuk, N.C.; Davis, F.F. Alteration of immunological properties of bovine serum albumin by covalent attachment of polyethylene glycol. *J. Biol. Chem.* **1977**, *252*, 3578–3581. [PubMed]
34. Piedmonte, D.M.; Treuheit, M.J. Formulation of Neulasta® (pegfilgrastim). *Adv. Drug Deliv. Rev.* **2008**, *60*, 50–58. [CrossRef] [PubMed]
35. Ettinger, A.R. Pegaspargase (Oncaspar). *J. Pediatric Oncol. Nurs.* **1995**, *12*, 46–48. [CrossRef] [PubMed]
36. Lang, L. FDA Approves Cimzia to Treat Crohn's Disease. *Gastroenterology* **2008**, *134*, 1819. [CrossRef] [PubMed]
37. Sánchez-Fructuoso, A.; Guirado, L.; Ruiz, J.C.; Torregrosa, V.; Gonzalez, E.; Suarez, M.L.; Galléego, R. Anemia control in kidney transplant patients treated with methoxy polyethylene glycol-epoetin beta (Mircera): The anemiatrans group. *Transplant. Proc.* **2010**, *42*, 2931–2934. [CrossRef]
38. Parfrey, P.S.; Warden, G.; Barrett, B.J. On peginesatide and anemia treatment in CKD. *Am. J. Kidney Dis.* **2013**, *62*, 659–661. [CrossRef]
39. Shukla, D.; Namperumalsamy, P.; Goldbaum, M.; Cunningham, E.T., Jr. Pegaptanib sodium for ocular vascular disease. *Indian J. Ophthalmol.* **2007**, *55*, 427–430. [PubMed]
40. Hoy, S.M. Peginterferon beta-1a: A review of its use in patients with relapsing-remitting multiple sclerosis. *CNS Drugs* **2015**, *29*, 171–179. [CrossRef] [PubMed]
41. Berhanu, A.A.; Krasnokutsky, S.; Keenan, R.T.; Pillinger, M.H. Pegloticase failure and a possible solution: Immunosuppression to prevent intolerance and inefficacy in patients with gout. *Semin. Arthritis Rheum.* **2017**, *46*, 754–758. [CrossRef] [PubMed]
42. Pasut, G.; Veronese, F.M. Polymer-drug conjugation, recent achievements and general strategies. *Prog. Polym. Sci.* **2007**, *32*, 933–961. [CrossRef]
43. Jevševar, S.; Kunstelj, M.; Porekar, V.G. PEGylation of therapeutic proteins. *Biotechnol. J.* **2010**, *5*, 113–128. [CrossRef] [PubMed]
44. Burdick, J.A.; Anseth, K.S. Photoencapsulation of osteoblasts in injectable RGD-modified PEG hydrogels for bone tissue engineering. *Biomaterials* **2002**, *23*, 4315–4323. [CrossRef]
45. Roberts, M.J.; Bentley, M.D.; Harris, J.M. Chemistry for peptide and protein PEGylation. *Adv. Drug Deliv. Rev.* **2002**, *54*, 459–476. [CrossRef]
46. Caliceti, P.; Veronese, F.M. Pharmacokinetic and biodistribution properties of poly(ethylene glycol)-protein conjugates. *Adv. Drug Deliv. Rev.* **2003**, *55*, 1261–1277. [CrossRef]
47. Manjula, B.N.; Tsai, A.; Upadhya, R.; Perumalsamy, K.; Smith, P.K.; Malavalli, A.; Vandegriff, K.; Winslow, R.M.; Intaglietta, M.; Prabhakaran, M.; et al. Site-specific PEGylation of hemoglobin at Cys-93(β): Correlation between the colligative properties of the PEGylated protein and the length of the conjugated PEG chain. *Bioconjugate Chem.* **2003**, *14*, 464–472. [CrossRef] [PubMed]
48. Meng, F.; Manjula, B.N.; Tsai, A.G.; Cabrales, P.; Intaglietta, M.; Smith, P.K.; Prabhakaran, M.; Acharya, S.A. Hexa-thiocarbamoyl phenyl PEG5K Hb: Vasoactivity and structure: The conjugation linkage on the pegylation induced plasma expander-like solution properties of PEG-Hb adducts. *Protein J.* **2009**, *28*, 199–212. [CrossRef] [PubMed]
49. Yang, C.; Lu, D.; Liu, Z. How PEGylation Enhances the Stability and Potency of Insulin: A Molecular Dynamics Simulation. *Biochemistry* **2011**, *50*, 2585–2593. [CrossRef]

50. Zhang, Y.; Han, K.; Lu, D.; Liu, Z. Reversible encapsulation of lysozyme within mPEG-b-PMAA: Experimental observation and molecular dynamics simulation. *Soft Matter* **2013**, *9*, 8723–8729. [CrossRef]
51. Chen, G.; Kong, X.; Zhu, J.; Lu, D.; Liu, Z. How ABA block polymers activate cytochrome c in toluene: Molecular dynamics simulation and experimental observation. *Phys. Chem. Chem. Phys.* **2015**, *17*, 10708–10714. [CrossRef] [PubMed]
52. Xue, Y.; O'Mara, M.L.; Surawski, P.P.T.; Trau, M.; Mark, A.E. Effect of poly(ethylene glycol) (PEG) spacers on the conformational properties of small peptides: A molecular dynamics study. *Langmuir* **2011**, *27*, 296–303. [CrossRef] [PubMed]
53. Mu, Q.; Hu, T.; Yu, J. Molecular Insight into the Steric Shielding Effect of PEG on the Conjugated Staphylokinase: Biochemical Characterization and Molecular Dynamics Simulation. *PLoS ONE* **2013**, *8*, e68559. [CrossRef] [PubMed]
54. Khameneh, B.; Jaafari, M.R.; Hassanzadeh-Khayyat, M.; Varasteh, A.; Chamani, J.; Iranshahi, M.; Mohammadpanah, H.; Abnous, K.; Saberi, M.R. Preparation, characterization and molecular modeling of PEGylated human growth hormone with agonist activity. *Int. J. Biol. Macromol.* **2015**, *80*, 400–409. [CrossRef] [PubMed]
55. Diaferia, C.; Sibillano, T.; Balasco, N.; Giannini, C.; Roviello, V.; Vitagliano, L.; Morelli, G.; Accardo, A. Hierarchical Analysis of Self-Assembled PEGylated Hexaphenylalanine Photoluminescent Nanostructures. *Chem. A Eur. J.* **2016**, *22*, 16586–16597. [CrossRef] [PubMed]
56. Diaferia, C.; Balasco, N.; Altamura, D.; Sibillano, T.; Gallo, E.; Roviello, V.; Giannini, C.; Morelli, G.; Vitagliano, L.; Accardo, A. Assembly modes of hexaphenylalanine variants as function of the charge states of their terminal ends. *Soft Matter* **2018**, *14*, 8219–8230. [CrossRef] [PubMed]
57. Diaferia, C.; Balasco, N.; Sibillano, T.; Giannini, C.; Vitagliano, L.; Morelli, G.; Accardo, A. Structural Characterization of Self-Assembled Tetra-Tryptophan Based Nanostructures: Variations on a Common Theme. *ChemPhysChem* **2018**, *19*, 1635–1642. [CrossRef]
58. Diaferia, C.; Balasco, N.; Sibillano, T.; Ghosh, M.; Adler-Abramovich, L.; Giannini, C.; Vitagliano, L.; Morelli, G.; Accardo, A. Amyloid-Like Fibrillary Morphology Originated by Tyrosine-Containing Aromatic Hexapeptides. *Chem. A Eur. J.* **2018**, *24*, 6804–6817. [CrossRef] [PubMed]
59. Settanni, G.; Zhou, J.; Schmid, F. Interactions between proteins and poly(ethylene-glycol) investigated using molecular dynamics simulations. *Proc. J. Phys. Conf. Ser.* **2017**, *921*, 012002. [CrossRef]
60. Settanni, G.; Zhou, J.; Suo, T.; Schöttler, S.; Landfester, K.; Schmid, F.; Mailänder, V. Protein corona composition of poly(ethylene glycol)-and poly (phosphoester)-coated nanoparticles correlates strongly with the amino acid composition of the protein surface. *Nanoscale* **2017**, *9*, 2138–2144. [CrossRef] [PubMed]
61. Settanni, G.; Schäfer, T.; Muhl, C.; Barz, M.; Schmid, F. Poly-sarcosine and Poly(Ethylene-Glycol) Interactions with Proteins Investigated Using Molecular Dynamics Simulations. *Comput. Struct. Biotechnol. J.* **2018**, *16*, 543–550. [CrossRef] [PubMed]
62. Kurinomaru, T.; Kuwada, K.; Tomita, S.; Kameda, T.; Shiraki, K. Noncovalent PEGylation through Protein-Polyelectrolyte Interaction: Kinetic Experiment and Molecular Dynamics Simulation. *J. Phys. Chem. B* **2017**, *121*, 6785–6791. [CrossRef] [PubMed]
63. Zaghmi, A.; Mendez-Villuendas, E.; Greschner, A.A.; Liu, J.Y.; de Haan, H.W.; Gauthier, M.A. Mechanisms of activity loss for a multi-PEGylated protein by experiment and simulation. *Mater. Today Chem.* **2019**, *12*, 121–131. [CrossRef]
64. Sindhu, R.; Pradeep, H.; Manonmani, H.K. Polyethylene glycol acts as a mechanistic stabilizer of L-asparaginase: A computational probing. *Med. Chem.* **2019**, *15*, 703–711. [CrossRef] [PubMed]
65. Ramezanghorbani, F.; Lin, P.; Colina, C.M. Optimizing Protein-Polymer Interactions in a Poly(ethylene glycol) Coarse-Grained Model. *J. Phys. Chem. B* **2018**, *122*, 7997–8005. [CrossRef]
66. Munasinghe, A.; Mathavan, A.; Lin, P.; Colina, C.M. PEGylation within a confined hydrophobic cavity of a protein. *Phys. Chem. Chem. Phys.* **2019**, *21*, 25584–25596. [CrossRef]
67. Baker, S.L.; Munasinghe, A.; Murata, H.; Lin, P.; Matyjaszewski, K.; Colina, C.M.; Russell, A.J. Intramolecular Interactions of Conjugated Polymers Mimic Molecular Chaperones to Stabilize Protein-Polymer Conjugates. *Biomacromolecules* **2018**, *19*, 3798–3813. [CrossRef]
68. Rukmani, S.J.; Anstine, D.M.; Munasinghe, A.; Colina, C.M. An Insight into Structural and Mechanical Properties of Ideal-Networked Poly(Ethylene Glycol)–Peptide Hydrogels from Molecular Dynamics Simulations. *Macromol. Chem. Phys.* **2020**, *221*, 1900326. [CrossRef]

69. Zasloff, M. Antimicrobial peptides of multicellular organisms. *Nature* **2002**, *415*, 389–395. [CrossRef] [PubMed]
70. Matsuzaki, K. Why and how are peptide-lipid interactions utilized for self-defense? Magainins and tachyplesins as archetypes. *Biochim. Biophys. Acta-Biomembr.* **1999**, *1462*, 1–10. [CrossRef]
71. Matsuzaki, K. Control of cell selectivity of antimicrobial peptides. *Biochim. Biophys. Acta-Biomembr.* **2009**, *1788*, 1687–1692. [CrossRef] [PubMed]
72. Guiotto, A.; Pozzobon, M.; Canevari, M.; Manganelli, R.; Scarin, M.; Veronese, F.M. PEGylation of the antimicrobial peptide nisin A: Problems and perspectives. *Farmaco* **2003**, *58*, 45–50. [CrossRef]
73. Imura, Y.; Nishida, M.; Matsuzaki, K. Action mechanism of PEGylated magainin 2 analogue peptide. *Biochim. Biophys. Acta-Biomembr.* **2007**, *1768*, 2578–2585. [CrossRef] [PubMed]
74. Imura, Y.; Nishida, M.; Ogawa, Y.; Takakura, Y.; Matsuzaki, K. Action mechanism of tachyplesin I and effects of PEGylation. *Biochim. Biophys. Acta-Biomembr.* **2007**, *1768*, 1160–1169. [CrossRef] [PubMed]
75. Singh, S.; Papareddy, P.; Mörgelin, M.; Schmidtchen, A.; Malmsten, M. Effects of PEGylation on Membrane and Lipopolysaccharide Interactions of Host Defense Peptides. *Biomacromolecules* **2014**, *15*, 1337–1345. [CrossRef] [PubMed]
76. Gong, Y.; Andina, D.; Nahar, S.; Leroux, J.C.; Gauthier, M.A. Releasable and traceless PEGylation of arginine-rich antimicrobial peptides. *Chem. Sci.* **2017**, *8*, 4082–4086. [CrossRef] [PubMed]
77. Morris, C.J.; Beck, K.; Fox, M.A.; Ulaeto, D.; Clark, G.C.; Gumbleton, M. Pegylation of antimicrobial peptides maintains the active peptide conformation, model membrane interactions, and antimicrobial activity while improving lung tissue biocompatibility following airway delivery. *Antimicrob. Agents Chemother.* **2012**, *56*, 3298–3308. [CrossRef]
78. Falciani, C.; Lozzi, L.; Scali, S.; Brunetti, J.; Bracci, L.; Pini, A. Site-specific pegylation of an antimicrobial peptide increases resistance to Pseudomonas aeruginosa elastase. *Amino Acids* **2014**, *46*, 1403–1407. [CrossRef]
79. Wu, X.; Chang, H.; Mello, C.; Nagarajan, R.; Narsimhan, G. Effect of interaction with coesite silica on the conformation of Cecropin P1 using explicit solvent molecular dynamics simulation. *J. Chem. Phys.* **2013**, *138*, 01B618. [CrossRef] [PubMed]
80. Wu, X.; Wei, P.H.; Zhu, X.; Wirth, M.J.; Bhunia, A.; Narsimhan, G. Effect of immobilization on the antimicrobial activity of a cysteine-terminated antimicrobial Peptide Cecropin P1 tethered to silica nanoparticle against E. coli O157:H7 EDL933. *Colloids Surf. B Biointerfaces* **2017**, *156*, 305–312. [CrossRef] [PubMed]
81. Han, E.; Lee, H. Effects of pegylation on the binding interaction of magainin 2 and tachyplesin I with lipid bilayer surface. *Langmuir* **2013**, *29*, 14214–14221. [CrossRef] [PubMed]
82. Jafari, M.; Doustdar, F.; Mehrnejad, F. Molecular Self-Assembly Strategy for Encapsulation of an Amphipathic α-Helical Antimicrobial Peptide into the Different Polymeric and Copolymeric Nanoparticles. *J. Chem. Inf. Modeling* **2019**, *59*, 550–563. [CrossRef] [PubMed]
83. Souza, F.R.; Souza, L.M.P.; Pimentel, A.S. Permeation of beta-defensin-3 encapsulated with polyethylene glycol in lung surfactant models at air-water interface. *Colloids Surf. B Biointerfaces* **2019**, *182*, 110357. [CrossRef] [PubMed]
84. Asadzadeh, H.; Moosavi, A.; Arghavani, J.H. The effect of chitosan and PEG polymers on stabilization of GF-17 structure: A molecular dynamics study. *Carbohydr. Polym.* **2020**, *237*, 116124. [CrossRef] [PubMed]
85. Lupas, A.N.; Gruber, M. The structure of alpha-helical coiled coils. In *Fibrous Proteins: Coiled-Coils, Collagen and Elastomers*; Elsevier Academic Press Inc.: San Diego, CA, USA, 2005; Volume 70, pp. 37–38.
86. Gruber, M.; Lupas, A.N. Historical review: Another 50th anniversary-new periodicities in coiled coils. *Trends Biochem. Sci.* **2003**, *28*, 679–685. [CrossRef] [PubMed]
87. Woolfson, D.N. The design of coiled-coil structures and assemblies. In *Fibrous Proteins: Coiled-Coils, Collagen and Elastomers*; Elsevier Academic Press Inc.: San Diego, CA, USA, 2005; Volume 70, pp. 79–112.
88. Woolfson, D.N.; Ryadnov, M.G. Peptide-based fibrous biomaterials: Some things old, new and borrowed. *Curr. Opin. Chem. Biol.* **2006**, *10*, 559–567. [CrossRef] [PubMed]
89. Vandermeulen, G.W.M.; Tziatzios, C.; Klok, H.A. Reversible self-organization of poly(ethylene glycol)-based hybrid block copolymers mediated by a de novo four-stranded α-helical coiled coil motif. *Macromolecules* **2003**, *36*, 4107–4114. [CrossRef]
90. Vandermeulen, G.W.M.; Hinderberger, D.; Xu, H.; Sheiko, S.S.; Jeschke, G.; Klok, H.A. Structure and dynamics of self-assembled poly(ethylene glycol) based coiled-coil nano-objects. *ChemPhysChem* **2004**, *5*, 488–494. [CrossRef] [PubMed]

91. Klok, H.A.; Vandermeulen, G.W.M.; Nuhn, H.; Rösler, A.; Hamley, I.W.; Castelletto, V.; Xu, H.; Sheiko, S.S. Peptide mediated formation of hierarchically organized solution and solid state polymer nanostructures. *Faraday Discuss.* **2005**, *128*, 29–41. [CrossRef] [PubMed]
92. Vandermeulen, G.W.M.; Tziatzios, C.; Duncan, R.; Klok, H.A. PEG-based hybrid block copolymers containing α-helical coiled coil peptide sequences: Control of self-assembly and preliminary biological evaluation. *Macromolecules* **2005**, *38*, 761–769. [CrossRef]
93. Deacon, S.P.E.; Apostolovic, B.; Carbajo, R.J.; Schott, A.K.; Beck, K.; Vicent, M.J.; Pineda-Lucena, A.; Klok, H.A.; Duncan, R. Polymer coiled-coil conjugates: Potential for development as a new class of therapeutic "molecular Switch". *Biomacromolecules* **2011**, *12*, 19–27. [CrossRef] [PubMed]
94. Marsden, H.R.; Korobko, A.V.; Van Leeuwen, E.N.M.; Pouget, E.M.; Veen, S.J.; Sommerdijk, N.A.J.M.; Kros, A. Noncovalent triblock copolymers based on a coiled-coil peptide motif. *J. Am. Chem. Soc.* **2008**, *130*, 9386–9393. [CrossRef]
95. Robson Marsden, H.; Handgraaf, J.W.; Nudelman, F.; Sommerdijk, N.A.J.M.; Kros, A. Uniting polypeptides with sequence-designed peptides: Synthesis and assembly of poly(γ-benzyl L-glutamate)-b-coiled-coil peptide copolymers. *J. Am. Chem. Soc.* **2010**, *132*, 2370–2377. [CrossRef] [PubMed]
96. Tomatsu, I.; Marsden, H.R.; Rabe, M.; Versluis, F.; Zheng, T.; Zope, H.; Kros, A. Influence of pegylation on peptide-mediated liposome fusion. *J. Mater. Chem.* **2011**, *21*, 18927–18933. [CrossRef]
97. Martelli, G.; Zope, H.R.; Bròvia Capell, M.; Kros, A. Coiled-coil peptide motifs as thermoresponsive valves for mesoporous silica nanoparticles. *Chem. Commun.* **2013**, *49*, 9932–9934. [CrossRef] [PubMed]
98. Zheng, T.; Voskuhl, J.; Versluis, F.; Zope, H.R.; Tomatsu, I.; Marsden, H.R.; Kros, A. Controlling the rate of coiled coil driven membrane fusion. *Chem. Commun.* **2013**, *49*, 3649–3651. [CrossRef] [PubMed]
99. Kong, L.; Askes, S.H.C.; Bonnet, S.; Kros, A.; Campbell, F. Temporal Control of Membrane Fusion through Photolabile PEGylation of Liposome Membranes. *Angew. Chem. Int. Ed.* **2016**, *55*, 1396–1400. [CrossRef] [PubMed]
100. Daudey, G.A.; Zope, H.R.; Voskuhl, J.; Kros, A.; Boyle, A.L. Membrane-Fusogen Distance Is Critical for Efficient Coiled-Coil-Peptide-Mediated Liposome Fusion. *Langmuir* **2017**, *33*, 12443–12452. [CrossRef] [PubMed]
101. Crone, N.S.A.; Minnee, D.; Kros, A.; Boyle, A.L. Peptide-mediated liposome fusion: The effect of anchor positioning. *Int. J. Mol. Sci.* **2018**, *19*, 211. [CrossRef] [PubMed]
102. Daudey, G.A.; Schwieger, C.; Rabe, M.; Kros, A. Influence of Membrane-Fusogen Distance on the Secondary Structure of Fusogenic Coiled Coil Peptides. *Langmuir* **2019**, *35*, 5501–5508. [CrossRef]
103. Mora, N.L.; Boyle, A.L.; Kolck, B.J.; Rossen, A.; Pokorná, Š.; Koukalová, A.; Šachl, R.; Hof, M.; Kros, A. Controlled Peptide-Mediated Vesicle Fusion Assessed by Simultaneous Dual-Colour Time-Lapsed Fluorescence Microscopy. *Sci. Rep.* **2020**, *10*, 1–13. [CrossRef] [PubMed]
104. Shu, J.Y.; Tan, C.; DeGrado, W.F.; Xu, T. New design of helix bundle peptide-polymer conjugates. *Biomacromolecules* **2008**, *9*, 2111–2117. [CrossRef] [PubMed]
105. Shu, J.Y.; Huang, Y.J.; Tan, C.; Presley, A.D.; Chang, J.; Xu, T. Amphiphilic peptide-polymer conjugates based on the coiled-coil helix bundle. *Biomacromolecules* **2010**, *11*, 1443–1452. [CrossRef] [PubMed]
106. Dong, H.; Dube, N.; Shu, J.Y.; Seo, J.W.; Mahakian, L.M.; Ferrara, K.W.; Xu, T. Long-circulating 15 nm micelles based on amphiphilic 3-helix peptide-peg conjugates. *ACS Nano* **2012**, *6*, 5320–5329. [CrossRef] [PubMed]
107. Dong, H.; Shu, J.Y.; Dube, N.; Ma, Y.; Tirrell, M.V.; Downing, K.H.; Xu, T. 3-Helix micelles stabilized by polymer springs. *J. Am. Chem. Soc.* **2012**, *134*, 11807–11814. [CrossRef] [PubMed]
108. Shu, J.Y.; Lund, R.; Xu, T. Solution structural characterization of coiled-coil peptide-polymer side-conjugates. *Biomacromolecules* **2012**, *13*, 1945–1955. [CrossRef] [PubMed]
109. Lund, R.; Shu, J.; Xu, T. A small-angle x-ray scattering study of α-helical bundle-forming peptide-polymer conjugates in solution: Chain conformations. *Macromolecules* **2013**, *46*, 1625–1632. [CrossRef]
110. Ang, J.; Ma, D.; Lund, R.; Keten, S.; Xu, T. Internal Structure of 15 nm 3-Helix Micelle Revealed by Small-Angle Neutron Scattering and Coarse-Grained MD Simulation. *Biomacromolecules* **2016**, *17*, 3262–3267. [CrossRef] [PubMed]
111. Ang, J.; Ma, D.; Jung, B.T.; Keten, S.; Xu, T. Sub-20 nm Stable Micelles Based on a Mixture of Coiled-Coils: A Platform for Controlled Ligand Presentation. *Biomacromolecules* **2017**, *18*, 3572–3580. [CrossRef] [PubMed]

112. Lund, R.; Ang, J.; Shu, J.Y.; Xu, T. Understanding Peptide Oligomeric State in Langmuir Monolayers of Amphiphilic 3-Helix Bundle-Forming Peptide-PEG Conjugates. *Biomacromolecules* **2016**, *17*, 3964–3972. [CrossRef] [PubMed]
113. Ang, J.; Jung, B.T.; Dong, H.; Xu, T. Kinetic Pathway of 3-Helix Micelle Formation. *Biomacromolecules* **2017**, *18*, 976–984. [CrossRef] [PubMed]
114. Jain, A.; Ashbaugh, H.S. Helix stabilization of poly(ethylene glycol)-peptide conjugates. *Biomacromolecules* **2011**, *12*, 2729–2734. [CrossRef] [PubMed]
115. Hamed, E.; Xu, T.; Keten, S. Poly(ethylene glycol) conjugation stabilizes the secondary structure of α-helices by reducing peptide solvent accessible surface area. *Biomacromolecules* **2013**, *14*, 4053–4060. [CrossRef] [PubMed]
116. Ruiz, L.; Keten, S. Directing the self-assembly of supra-biomolecular nanotubes using entropic forces. *Soft Matter* **2014**, *10*, 851–861. [CrossRef] [PubMed]
117. Hamed, E.; Ma, D.; Keten, S. Multiple PEG Chains Attached onto the Surface of a Helix Bundle: Conformations and Implications. *ACS Biomater. Sci. Eng.* **2015**, *1*, 79–84. [CrossRef]
118. Ma, D.; DeBenedictis, E.P.; Lund, R.; Keten, S. Design of polymer conjugated 3-helix micelles as nanocarriers with tunable shapes. *Nanoscale* **2016**, *8*, 19334–19342. [CrossRef]
119. Ma, D.; Keten, S. Stable micelles based on a mixture of coiled-coils: The role of different oligomeric states. *Nanoscale* **2018**, *10*, 7589–7596. [CrossRef]
120. Woo, S.Y.; Lee, H. Molecular dynamics studies of PEGylated α-helical coiled coils and their self-assembled micelles. *Langmuir* **2014**, *30*, 8848–8855. [CrossRef]
121. Gregoriadis, G. The carrier potential of liposomes in biology and medicine (first of two parts). *N. Engl. J. Med.* **1976**, *295*, 704–710. [CrossRef]
122. Weinstein, J.N.; Yoshikami, S.; Henkart, P.; Blumenthal, R.; Hagins, W.A. Liposome-cell interaction: Transfer and intracellular release of a trapped fluorescent marker. *Science* **1977**, *195*, 489–492. [CrossRef] [PubMed]
123. Yatvin, M.B.; Weinstein, J.N.; Dennis, W.H.; Blumenthal, R. Design of liposomes for enhanced local release of drugs by hyperthermia. *Science* **1978**, *202*, 1290–1293. [CrossRef] [PubMed]
124. Barenholz, Y.; Bolotin, E.; Cohen, R.; Gabizon, A. Sterically stabilized doxorubicin loaded liposomes (DOX-SL^{TM}): From basics to the clinics. *Phosphorus Sulfur Silicon Relat. Elem.* **1996**, *109*, 293–296. [CrossRef]
125. Hristova, K.; Kenworthy, A.; McIntosh, T.J. Effect Of Bilayer Composition on the Phase-Behavior of Liposomal Suspensions Containing Poly(ethylene glycol)-Lipids. *Macromolecules* **1995**, *28*, 7693–7699. [CrossRef]
126. Kenworthy, A.K.; Simon, S.A.; McIntosh, T.J. Structure and Phase-Behavior of Lipid Suspensions Containing Phospholipids with Covalently Attached Poly(Ethylene Glycol). *Biophys. J.* **1995**, *68*, 1903–1920. [CrossRef]
127. Needham, D.; Hristova, K.; McIntosh, T.J.; Dewhirst, M.; Wu, N.; Lasic, D.D.; Alving, C.R.; Wassef, N.M.; Senior, J.H.; Ghosh, P.C.; et al. Polymer-grafted liposomes: Physical basis for the 'Stealth' property. *J. Liposome Res.* **1992**, *2*, 411–430. [CrossRef]
128. Needham, D.; McIntosh, T.J.; Lasic, D.D. Repulsive Interactions and Mechanical Stability of Polymer-Grafted Lipid-Membranes. *Biochim. Biophys. Acta* **1992**, *1108*, 40–48. [CrossRef]
129. Kenworthy, A.K.; Hristova, K.; Needham, D.; McIntosh, T.J. Range and Magnitude of the Steric Pressure Between Bilayers Containing Phospholipids with Covalently Attached Poly(Ethylene Glycol). *Biophys. J.* **1995**, *68*, 1921–1936. [CrossRef]
130. Kuhl, T.L.; Leckband, D.E.; Lasic, D.D.; Israelachvili, J.N. Modulation of interaction forces between bilayers exposing short-chained ethylene oxide headgroups. *Biophys. J.* **1994**, *66*, 1479–1488. [CrossRef]
131. Du, H.; Chandaroy, P.; Hui, S.W. Grafted poly-(ethylene glycol) on lipid surface inhibits protein adsorption and cell adhesion. *Biochim. Biophys. Acta-Biomembr.* **1997**, *1326*, 236–248. [CrossRef]
132. Efremova, N.V.; Bondurant, B.; O'Brien, D.F.; Leckband, D.E. Measurements of interbilayer forces and protein adsorption on uncharged lipid bilayers displaying poly(ethylene glycol) chains. *Biochemistry* **2000**, *39*, 3441–3451. [CrossRef]
133. Bartucci, R.; Pantusa, M.; Marsh, D.; Sportelli, L. Interaction of human serum albumin with membranes containing polymer-grafted lipids: Spin-label ESR studies in the mushroom and brush regimes. *Biochim. Biophys. Acta-Biomembr.* **2002**, *1564*, 237–242. [CrossRef]
134. Chiu, G.N.C.; Bally, M.B.; Mayer, L.D. Selective protein interactions with phosphatidylserine containing liposomes alter the steric stabilization properties of poly(ethylene glycol). *Biochim. Biophys. Acta-Biomembr.* **2001**, *1510*, 56–69. [CrossRef]

135. Li, W.M.; Mayer, L.D.; Bally, M.B. Prevention of antibody-mediated elimination of ligand-targeted liposomes by using poly(ethylene glycol)-modified lipids. *J. Pharmacol. Exp. Ther.* **2002**, *300*, 976–983. [CrossRef] [PubMed]
136. Dos Santos, N.; Allen, C.; Doppen, A.M.; Anantha, M.; Cox, K.A.K.; Gallagher, R.C.; Karlsson, G.; Edwards, K.; Kenner, G.; Samuels, L.; et al. Influence of poly(ethylene glycol) grafting density and polymer length on liposomes: Relating plasma circulation lifetimes to protein binding. *Biochim. Biophys. Acta-Biomembr.* **2007**, *1768*, 1367–1377. [CrossRef]
137. Gref, R.; Lück, M.; Quellec, P.; Marchand, M.; Dellacherie, E.; Harnisch, S.; Blunk, T.; Müller, R.H. 'Stealth' corona-core nanoparticles surface modified by polyethylene glycol (PEG): Influences of the corona (PEG chain length and surface density) and of the core composition on phagocytic uptake and plasma protein adsorption. *Colloids Surf. B Biointerfaces* **2000**, *18*, 301–313. [CrossRef]
138. Perry, J.L.; Reuter, K.G.; Kai, M.P.; Herlihy, K.P.; Jones, S.W.; Luft, J.C.; Napier, M.; Bear, J.E.; Desimone, J.M. PEGylated PRINT nanoparticles: The impact of PEG density on protein binding, macrophage association, biodistribution, and pharmacokinetics. *Nano Lett.* **2012**, *12*, 5304–5310. [CrossRef] [PubMed]
139. Schneck, E.; Berts, I.; Halperin, A.; Daillant, J.; Fragneto, G. Neutron reflectometry from poly (ethylene-glycol) brushes binding anti-PEG antibodies: Evidence of ternary adsorption. *Biomaterials* **2015**, *46*, 95–104. [CrossRef] [PubMed]
140. Torchilin, V.P.; Klibanov, A.L.; Huang, L.; Odonnell, S.; Nossiff, N.D.; Khaw, B.A. Targeted Accumulation of Polyethylene Glycol-Coated Immunoliposomes In Infarcted Rabbit Myocardium. *FASEB J.* **1992**, *6*, 2716–2719. [CrossRef] [PubMed]
141. de Gennes, P.G. Polymers at An Interface—A Simplified View. *Adv. Colloid Interface Sci.* **1987**, *27*, 189–209. [CrossRef]
142. Jeon, S.I.; Lee, J.H.; Andrade, J.D.; De Gennes, P.G. Protein-surface interactions in the presence of polyethylene oxide. I. Simplified theory. *J. Colloid Interface Sci.* **1991**, *142*, 149–158. [CrossRef]
143. Jeon, S.I.; Andrade, J.D. Protein-surface interactions in the presence of polyethylene oxide. II. Effect of protein size. *J. Colloid Interface Sci.* **1991**, *142*, 159–166. [CrossRef]
144. Szleifer, I. Protein adsorption on surfaces with grafted polymers: A theoretical approach. *Biophys. J.* **1997**, *72*, 595–612. [CrossRef]
145. Halperin, A. Polymer brushes that resist adsorption of model proteins: Design parameters. *Langmuir* **1999**, *15*, 2525–2533. [CrossRef]
146. Halperin, A.; Kröger, M. Ternary protein adsorption onto brushes: Strong versus weak. *Langmuir* **2009**, *25*, 11621–11634. [CrossRef] [PubMed]
147. Taylor, W.; Jones, R.A.L. Protein adsorption on well-characterized polyethylene oxide brushes on gold: Dependence on molecular weight and grafting density. *Langmuir* **2013**, *29*, 6116–6122. [CrossRef] [PubMed]
148. Pal, S.; Milano, G.; Roccatano, D. Synthetic Polymers and Biomembranes. How Do They Interact? Atomistic Molecular Dynamics Simulation Study of PEO in Contact with a DMPC Lipid Bilayer. *J. Phys. Chem. B* **2006**, *110*, 26170–26179. [CrossRef] [PubMed]
149. Samanta, S.; Hezaveh, S.; Roccatano, D. Theoretical Study of Binding and Permeation of Ether-Based Polymers through Interfaces. *J. Phys. Chem. B* **2013**, *117*, 14723–14731. [CrossRef]
150. Magarkar, A.; Karakas, E.; Stepniewski, M.; Róg, T.; Bunker, A. Molecular dynamics simulation of PEGylated bilayer interacting with salt ions: A model of the liposome surface in the bloodstream. *J. Phys. Chem. B* **2012**, *116*, 4212–4219. [CrossRef] [PubMed]
151. Lehtinen, J.; Magarkar, A.; Stepniewski, M.; Hakola, S.; Bergman, M.; Róg, T.; Yliperttula, M.; Urtti, A.; Bunker, A. Analysis of cause of failure of new targeting peptide in PEGylated liposome: Molecular modeling as rational design tool for nanomedicine. *Eur. J. Pharm. Sci.* **2012**, *46*, 121–130. [CrossRef]
152. Rissanen, S.; Kumorek, M.; Martinez-Seara, H.; Li, Y.C.; Jamróz, D.; Bunker, A.; Nowakowska, M.; Vattulainen, I.; Kepczynski, M.; Róg, T. Effect of PEGylation on drug entry into lipid bilayer. *J. Phys. Chem. B* **2014**, *118*, 144–151. [CrossRef]
153. Magarkar, A.; Róg, T.; Bunker, A. Molecular dynamics simulation of PEGylated membranes with cholesterol: Building toward the DOXIL formulation. *J. Phys. Chem. C* **2014**, *118*, 15541–15549. [CrossRef]
154. Dzieciuch, M.; Rissanen, S.; Szydłowska, N.; Bunker, A.; Kumorek, M.; Jamróz, D.; Vattulainen, I.; Nowakowska, M.; Róg, T.; Kepczynski, M. Pegylated liposomes as carriers of hydrophobic porphyrins. *J. Phys. Chem. B* **2015**, *119*, 6646–6657. [CrossRef] [PubMed]

155. Lajunen, T.; Kontturi, L.S.; Viitala, L.; Manna, M.; Cramariuc, O.; Róg, T.; Bunker, A.; Laaksonen, T.; Viitala, T.; Murtomäki, L.; et al. Indocyanine Green-Loaded Liposomes for Light-Triggered Drug Release. *Mol. Pharm.* **2016**, *13*, 2095–2107. [CrossRef] [PubMed]
156. Dzieciuch-Rojek, M.; Poojari, C.; Bednar, J.; Bunker, A.; Kozik, B.; Nowakowska, M.; Vattulainen, I.; Wydro, P.; Kepczynski, M.; Roǵ, T. Effects of membrane PEGylation on entry and location of antifungal drug itraconazole and their pharmacological implications. *Mol. Pharm.* **2017**, *14*, 1057–1070. [CrossRef] [PubMed]
157. Wilkosz, N.; Rissanen, S.; Cyza, M.; Szybka, R.; Nowakowska, M.; Bunker, A.; Róg, T.; Kepczynski, M. Effect of piroxicam on lipid membranes: Drug encapsulation and gastric toxicity aspects. *Eur. J. Pharm. Sci.* **2017**, *100*, 116–125. [CrossRef]
158. Lajunen, T.; Nurmi, R.; Wilbie, D.; Ruoslahti, T.; Johansson, N.G.; Korhonen, O.; Rog, T.; Bunker, A.; Ruponen, M.; Urtti, A. The effect of light sensitizer localization on the stability of indocyanine green liposomes. *J. Control. Release* **2018**, *284*, 213–223. [CrossRef]
159. Mastrotto, F.; Brazzale, C.; Bellato, F.; De Martin, S.; Grange, G.; Mahmoudzadeh, M.; Magarkar, A.; Bunker, A.; Salmaso, S.; Caliceti, P. In Vitro and in Vivo Behavior of Liposomes Decorated with PEGs with Different Chemical Features. *Mol. Pharm.* **2020**, *17*, 472–487. [CrossRef] [PubMed]
160. Srinivas, G.; Shelley, J.C.; Nielsen, S.O.; Discher, D.E.; Klein, M.L. Simulation of diblock copolymer self-assembly, using a coarse-grain model. *J. Phys. Chem. B* **2004**, *108*, 8153–8160. [CrossRef]
161. Srinivas, G.; Klein, M.L. Coarse-grain molecular dynamics simulations of diblock copolymer surfactants interacting with a lipid bilayer. *Mol. Phys.* **2004**, *102*, 883–889. [CrossRef]
162. Shinoda, W.; Discher, D.E.; Klein, M.L.; Loverde, S.M. Probing the structure of PEGylated-lipid assemblies by coarse-grained molecular dynamics. *Soft Matter* **2013**, *9*, 11549–11556. [CrossRef]
163. Marrink, S.J.; de Vries, A.H.; Mark, A.E. Coarse grained model for semiquantitative lipid simulations. *J. Phys. Chem. B* **2004**, *108*, 750–760. [CrossRef]
164. Marrink, S.J.; Risselada, H.J.; Yefimov, S.; Tieleman, D.P.; de Vries, A.H. The MARTINI force field: Coarse grained model for biomolecular simulations. *J. Phys. Chem. B* **2007**, *111*, 7812–7824. [CrossRef]
165. Yang, S.-C.; Faller, R. Pressure and Surface Tension Control Self-Assembled Structures in Mixtures of Pegylated and Non-Pegylated Lipids. *Langmuir* **2012**, *28*, 2275–2280. [CrossRef] [PubMed]
166. Hezaveh, S.; Samanta, S.; De Nicola, A.; Milano, G.; Roccatano, D. Understanding the Interaction of Block Copolymers with DMPC Lipid Bilayer Using Coarse-Grained Molecular Dynamics Simulations. *J. Phys. Chem. B* **2012**, *116*, 14333–14345. [CrossRef] [PubMed]
167. Lee, H.; Pastor, R.W. Coarse-Grained Model for PEGylated Lipids: Effect of PEGylation on the Size and Shape of Self-Assembled Structures. *J. Phys. Chem. B* **2011**, *115*, 7830–7837. [CrossRef]
168. Lee, H.; Larson, R.G. Adsorption of Plasma Proteins onto PEGylated Lipid Bilayers: The Effect of PEG Size and Grafting Density. *Biomacromolecules* **2016**, *17*, 1757–1765. [CrossRef]
169. Viitala, L.; Pajari, S.; Gentile, L.; Määttä, J.; Gubitosi, M.; Deska, J.; Sammalkorpi, M.; Olsson, U.; Murtomäki, L. Shape and Phase Transitions in a PEGylated Phospholipid System. *Langmuir* **2019**, *35*, 3999–4010. [CrossRef]
170. Vuorte, M.; Määttä, J.; Sammalkorpi, M. Simulations Study of Single-Component and Mixed n -Alkyl-PEG Micelles. *J. Phys. Chem. B* **2018**, *122*, 4851–4860. [CrossRef] [PubMed]
171. Majoros, I.J.; Williams, C.R.; Baker, J.R. Current dendrimer applications in cancer diagnosis and therapy. *Curr. Top. Med. Chem.* **2008**, *8*, 1165–1179. [CrossRef] [PubMed]
172. Tully, D.C.; Frechet, J.M.J. Dendrimers at surfaces and interfaces: Chemistry and applications. *Chem. Commun.* **2001**, 1229–1239. [CrossRef]
173. Gupta, U.; Agashe, H.B.; Asthana, A.; Jain, N.K. Dendrimers: Novel polymeric nanoarchitectures for solubility enhancement. *Biomacromolecules* **2006**, *7*, 649–658. [CrossRef] [PubMed]
174. Gillies, E.R.; Frechet, J.M.J. Dendrimers and dendritic polymers in drug delivery. *Drug Discov. Today* **2005**, *10*, 35–43. [CrossRef]
175. Tanis, I.; Karatasos, K. Molecular dynamics simulations of polyamidoamine dendrimers and their complexes with linear poly(ethylene oxide) at different pH conditions: Static properties and hydrogen bonding. *Phys. Chem. Chem. Phys.* **2009**, *11*, 10017–10028. [CrossRef] [PubMed]
176. Karatasos, K. Self-association and complexation of the anti-cancer drug doxorubicin with PEGylated hyperbranched polyesters in an aqueous environment. *J. Phys. Chem. B* **2013**, *117*, 2564–2575. [CrossRef] [PubMed]

177. Lee, H.; Larson, R.G. Molecular Dynamics Study of the Structure and Interparticle Interactions of Polyethylene Glycol-Conjugated PAMAM Dendrimers. *J. Phys. Chem. B* **2009**, *113*, 13202–13207. [CrossRef]
178. Lee, H.; Larson, R.G. Membrane Pore Formation Induced by Acetylated and Polyethylene Glycol-Conjugated Polyamidoamine Dendrimers. *J. Phys. Chem. C* **2011**, *115*, 5316–5322. [CrossRef]
179. Lee, H.; Larson, R.G. Effects of PEGylation on the Size and Internal Structure of Dendrimers: Self-Penetration of Long PEG Chains into the Dendrimer Core. *Macromolecules* **2011**, *44*, 2291–2298. [CrossRef]
180. Albertazzi, L.; Mickler, F.M.; Pavan, G.M.; Salomone, F.; Bardi, G.; Panniello, M.; Amir, E.; Kang, T.; Killops, K.L.; Bräuchle, C.; et al. Enhanced bioactivity of internally functionalized cationic dendrimers with PEG cores. *Biomacromolecules* **2012**, *13*, 4089–4097. [CrossRef]
181. Pavan, G.M.; Barducci, A.; Albertazzi, L.; Parrinello, M. Combining metadynamics simulation and experiments to characterize dendrimers in solution. *Soft Matter* **2013**, *9*, 2593–2597. [CrossRef]
182. Tintaru, A.; Chendo, C.; Wang, Q.; Viel, S.; Quéléver, G.; Peng, L.; Posocco, P.; Pricl, S.; Charles, L. Conformational sensitivity of conjugated poly(ethylene oxide)-poly(amidoamine) molecules to cations adducted upon electrospray ionization—A mass spectrometry, ion mobility and molecular modeling study. *Anal. Chim. Acta* **2014**, *808*, 163–174. [CrossRef]
183. Lin, X.; Bai, T.; Zuo, Y.Y.; Gu, N. Promote potential applications of nanoparticles as respiratory drug carrier: Insights from molecular dynamics simulations. *Nanoscale* **2014**, *6*, 2759–2767. [CrossRef]
184. Lim, J.; Lo, S.-T.; Hill, S.; Pavan, G.M.; Sun, X.; Simanek, E.E. Antitumor Activity and Molecular Dynamics Simulations of Paclitaxel-Laden Triazine Dendrimers. *Mol. Pharm.* **2012**, *9*, 404–412. [CrossRef]
185. Barraza, L.F.; Jiménez, V.A.; Alderete, J.B. Association of Methotrexate with Native and PEGylated PAMAM-G4 Dendrimers: Effect of the PEGylation Degree on the Drug-Loading Capacity and Preferential Binding Sites. *J. Phys. Chem. B* **2017**, *121*, 4–12. [CrossRef] [PubMed]
186. Sampogna-Mireles, D.; Araya-Durán, I.D.; Márquez-Miranda, V.; Valencia-Gallegos, J.A.; González-Nilo, F.D. Structural analysis of binding functionality of folic acid-PEG dendrimers against folate receptor. *J. Mol. Graph. Model.* **2017**, *72*, 201–208. [CrossRef]
187. Hsu, H.-J.; Han, Y.; Cheong, M.; Král, P.; Hong, S. Dendritic PEG outer shells enhance serum stability of polymeric micelles. *Nanomed. Nanotechnol. Biol. Med.* **2018**, *14*, 1879–1889. [CrossRef]
188. Diaz, C.; Benitez, C.; Vidal, F.; Barraza, L.F.; Jiménez, V.A.; Guzman, L.; Fuentealba, J.; Yevenes, G.E.; Alderete, J.B. Cytotoxicity and in vivo plasma kinetic behavior of surface-functionalized PAMAM dendrimers. *Nanomed. Nanotechnol. Biol. Med.* **2018**, *14*, 2227–2234. [CrossRef] [PubMed]
189. Wang, B.; Sun, Y.; Davis, T.P.; Ke, P.C.; Wu, Y.; Ding, F. Understanding Effects of PAMAM Dendrimer Size and Surface Chemistry on Serum Protein Binding with Discrete Molecular Dynamics Simulations. *ACS Sustain. Chem. Eng.* **2018**, *6*, 11704–11715. [CrossRef] [PubMed]
190. Bianco, A.; Kostarelos, K.; Prato, M. Applications of carbon nanotubes in drug delivery. *Curr. Opin. Chem. Biol.* **2005**, *9*, 674–679. [CrossRef]
191. Lacerda, L.; Bianco, A.; Prato, M.; Kostarelos, K. Carbon nanotubes as nanomedicines: From toxicology to pharmacology. *Adv. Drug Deliv. Rev.* **2006**, *58*, 1460–1470. [CrossRef]
192. Liu, Z.; Robinson, J.T.; Tabakman, S.M.; Yang, K.; Dai, H. Carbon materials for drug delivery & cancer therapy. *Mater. Today* **2011**, *14*, 316–323.
193. Ke, P.C.; Lamm, M.H. A biophysical perspective of understanding nanoparticles at large. *Phys. Chem. Chem. Phys.* **2011**, *13*, 7273–7283. [CrossRef] [PubMed]
194. Lin, S.; Keskar, G.; Wu, Y.; Wang, X.; Mount, A.S.; Klaine, S.J.; Moore, J.M.; Rao, A.M.; Ke, P.C. Detection of phospholipid-carbon nanotube translocation using fluorescence energy transfer. *Appl. Phys. Lett.* **2006**, *89*, 143118. [CrossRef]
195. Qiao, R.; Ke, P.C. Lipid-carbon nanotube self-assembly in aqueous solution. *J. Am. Chem. Soc.* **2006**, *128*, 13656–13657. [CrossRef] [PubMed]
196. Wu, Y.; Hudson, J.S.; Lu, Q.; Moore, J.M.; Mount, A.S.; Rao, A.M.; Alexov, E.; Ke, P.C. Coating single-walled carbon nanotubes with phospholipids. *J. Phys. Chem. B* **2006**, *110*, 2475–2478. [CrossRef] [PubMed]
197. Liu, Z.; Robinson, J.T.; Sun, X.; Dai, H. PEGylated nanographene oxide for delivery of water-insoluble cancer drugs. *J. Am. Chem. Soc.* **2008**, *130*, 10876–10877. [CrossRef]
198. Liu, X.; Tao, H.; Yang, K.; Zhang, S.; Lee, S.T.; Liu, Z. Optimization of surface chemistry on single-walled carbon nanotubes for in vivo photothermal ablation of tumors. *Biomaterials* **2011**, *32*, 144–151. [CrossRef]

199. Kam, N.W.S.; Liu, Z.; Dai, H. Functionalization of carbon nanotubes via cleavable disulfide bonds for efficient intracellular delivery of siRNA and potent gene silencing. *J. Am. Chem. Soc.* **2005**, *127*, 12492–12493. [CrossRef] [PubMed]
200. Mahajan, S.; Patharkar, A.; Kuche, K.; Maheshwari, R.; Deb, P.K.; Kalia, K.; Tekade, R.K. Functionalized carbon nanotubes as emerging delivery system for the treatment of cancer. *Int. J. Pharm.* **2018**, *548*, 540–558. [CrossRef] [PubMed]
201. Uddin, N.M.; Capaldi, F.M.; Farouk, B. Molecular dynamics simulations of the interactions and dispersion of carbon nanotubes in polyethylene oxide/water systems. *Polymer* **2011**, *52*, 288–296. [CrossRef]
202. Lee, H.; Kim, H. Self-assembly of lipids and single-walled carbon nanotubes: Effects of lipid structure and PEGylation. *J. Phys. Chem. C* **2012**, *116*, 9327–9333. [CrossRef]
203. Lee, H. Molecular Dynamics Studies of PEGylated Single-Walled Carbon Nanotubes: The Effect of PEG Size and Grafting Density. *J. Phys. Chem. C* **2013**, *117*, 26334–26341. [CrossRef]
204. Di Crescenzo, A.; Aschi, M.; Fontana, A. Toward a better understanding of steric stabilization when using block copolymers as stabilizers of single-walled carbon nanotubes (SWCNTs) aqueous dispersions. *Macromolecules* **2012**, *45*, 8043–8050. [CrossRef]
205. Aslan, S.; Määttä, J.; Haznedaroglu, B.Z.; Goodman, J.P.M.; Pfefferle, L.D.; Elimelech, M.; Pauthe, E.; Sammalkorpi, M.; Van Tassel, P.R. Carbon nanotube bundling: Influence on layer-by-layer assembly and antimicrobial activity. *Soft Matter* **2013**, *9*, 2136–2144. [CrossRef]
206. Sarukhanyan, E.; Milano, G.; Roccatano, D. Coating mechanisms of single-walled carbon nanotube by linear polyether surfactants: Insights from computer simulations. *J. Phys. Chem. C* **2014**, *118*, 18069–18078. [CrossRef]
207. Han, Y.; Ahn, S.K.; Zhang, Z.; Smith, G.S.; Do, C. Tunable Encapsulation Structure of Block Copolymer Coated Single-Walled Carbon Nanotubes in Aqueous Solution. *Macromolecules* **2015**, *48*, 3475–3480. [CrossRef]
208. Määttä, J.; Vierros, S.; Van Tassel, P.R.; Sammalkorpi, M. Size-selective, noncovalent dispersion of carbon nanotubes by PEGylated lipids: A coarse-grained molecular dynamics study. *J. Chem. Eng. Data* **2014**, *59*, 3080–3089. [CrossRef]
209. Skandani, A.A.; Al-Haik, M. Reciprocal effects of the chirality and the surface functionalization on the drug delivery permissibility of carbon nanotubes. *Soft Matter* **2013**, *9*, 11645–11649. [CrossRef] [PubMed]
210. Skandani, A.A.; Zeineldin, R.; Al-Haik, M. Effect of chirality and length on the penetrability of single-walled carbon nanotubes into lipid bilayer cell membranes. *Langmuir* **2012**, *28*, 7872–7879. [CrossRef] [PubMed]
211. Lee, H. Interparticle dispersion, membrane curvature, and penetration induced by single-walled carbon nanotubes wrapped with lipids and PEGylated lipids. *J. Phys. Chem. B* **2013**, *117*, 1337–1344. [CrossRef] [PubMed]
212. Lee, H. Adsorption of plasma proteins onto PEGylated single-walled carbon nanotubes: The effects of protein shape, PEG size and grafting density. *J. Mol. Graph. Model.* **2017**, *75*, 1–8. [CrossRef] [PubMed]
213. Lin, S.; Zhang, J.; Strano, M.S.; Blankschtein, D. Understanding selective molecular recognition in integrated carbon nanotube-polymer sensors by simulating physical analyte binding on carbon nanotube-polymer scaffolds. *Soft Matter* **2014**, *10*, 5991–6004. [CrossRef] [PubMed]
214. Hashemzadeh, H.; Raissi, H. The functionalization of carbon nanotubes to enhance the efficacy of the anticancer drug paclitaxel: A molecular dynamics simulation study. *J. Mol. Modeling* **2017**, *23*, 222. [CrossRef] [PubMed]
215. Kavyani, S.; Dadvar, M.; Modarress, H.; Amjad-Iranagh, S. A coarse grained molecular dynamics simulation study on the structural properties of carbon nanotube-dendrimer composites. *Soft Matter* **2018**, *14*, 3151–3163. [CrossRef]
216. Wolski, P.; Nieszporek, K.; Panczyk, T. Pegylated and folic acid functionalized carbon nanotubes as pH controlled carriers of doxorubicin. Molecular dynamics analysis of the stability and drug release mechanism. *Phys. Chem. Chem. Phys.* **2017**, *19*, 9300–9312. [CrossRef] [PubMed]
217. Wolski, P.; Nieszporek, K.; Panczyk, T. Multimodal, pH Sensitive, and Magnetically Assisted Carrier of Doxorubicin Designed and Analyzed by Means of Computer Simulations. *Langmuir* **2018**, *34*, 2543–2550. [CrossRef] [PubMed]
218. Meran, M.; Akkus, P.D.; Kurkcuoglu, O.; Baysak, E.; Hizal, G.; Haciosmanoglu, E.; Unlu, A.; Karatepe, N.; Güner, F.S. Noncovalent Pyrene-Polyethylene Glycol Coatings of Carbon Nanotubes Achieve in Vitro Biocompatibility. *Langmuir* **2018**, *34*, 12071–12082. [CrossRef] [PubMed]

219. Saberinasab, A.; Raissi, H.; Hashemzadeh, H. Understanding the effect of vitamin B6 and PEG functionalization on improving the performance of carbon nanotubes in temozolomide anticancer drug transportation. *J. Phys. D: Appl. Phys.* **2019**, *52*, 395402. [CrossRef]
220. Moradnia, H.; Raissi, H.; Shahabi, M. The performance of the single-walled carbon nanotube covalently modified with polyethylene glycol to delivery of Gemcitabine anticancer drug in the aqueous environment. *J. Biomol. Struct. Dyn.* **2020**. [CrossRef] [PubMed]
221. Lee, H. Effects of Nanoparticle Electrostatics and Protein–Protein Interactions on Corona Formation: Conformation and Hydrodynamics. *Small* **2020**, *16*, 1906598. [CrossRef] [PubMed]
222. Ingólfsson, H.I.; Melo, M.N.; van Eerden, F.J.; Arnarez, C.; Lopez, C.A.; Wassenaar, T.A.; Periole, X.; de Vries, A.H.; Tieleman, D.P.; Marrink, S.J. Lipid Organization of the Plasma Membrane. *J. Am. Chem. Soc.* **2014**, *136*, 14554–14559. [CrossRef] [PubMed]
223. Goga, N.; Melo, M.N.; Rzepiela, A.J.; De Vries, A.H.; Hadar, A.; Marrink, S.J.; Berendsen, H.J.C. Benchmark of schemes for multiscale molecular dynamics simulations. *J. Chem. Theory Comput.* **2015**, *11*, 1389–1398. [CrossRef] [PubMed]